CYCLOPs: A Unified Framework for Surface Flux-Driven Cyclones Outside the Tropics

Kerry Emanuel (1), Tommaso Alberti (2), Stella Bourdin (3), Suzana J. Camargo (4,5), Davide Faranda (6,7,8), Emmanouil Flaounas (9,10), Juan Jesus Gonzalez-Aleman (11), Chia-Ying Lee (4), Mario Marcello Miglietta (12), Claudia Pasquero (13), Alice Portal (14), Hamish Ramsay (15), Marco Reale (16), Romualdo Romero (17)

(1) Massachusetts Institute of Technology, 77 Mass. Ave., Cambridge, MA 02139

(2) Istituto Nazionale di Geofisica e Vulcanologia, Rome, Italy

(3) Atmospheric, Oceanic and Planetary Physics, Department of Physics, University of Oxford, Oxford, United Kingdom

(4) Lamont-Doherty Earth Observatory, Columbia University, Palisades, New York, USA

(5) Columbia Climate School, Columbia University, New York, New York, USA

(6) Laboratoire des Sciences du Climat et de l'Environnement, UMR 8212 CEA-CNRS-UVSQ, Université Paris-Saclay & IPSL, CE Saclay l'Orme des Merisiers, 91191 Gif-sur-Yvette, France

(7) London Mathematical Laboratory, 8 Margravine Gardens, London W6 8RH, UK

(8) LMD/IPSL, ENS, Université PSL, École Polytechnique, Institut Polytechnique de Paris, Sorbonne Université, CNRS, Paris France

(9) Institute for Atmospheric and Climate Science, ETH Zurich, Zurich, Switzerland

(10) Institute of Oceanography, Hellenic Centre for Marine Research, Athens, Greece

(11) Spanish State Meteorological Agency, AEMET, Department Development and Applications

(12) CNR-ISAC, Padua, Italy

(12) Spanish State Meteorological Agency, AEMET, Department Development and Applications

(13) Department of Earth and Environmental Sciences, University of Milano - Bicocca, Italy

(14) Institute of Atmospheric Sciences and Climate (CNR-ISAC), National Research Council of Italy, Bologna, Italy

(15) CSIRO Environment, Aspendale, Victoria, Australia

(16) National Institute of Oceanography and Applied Geophysics - OGS, Trieste, Italy

(17) Grup de Meteorologia, Departament de Física, Universitat de les Illes Balears, Palma de Mallorca, Spain

30   Correspondence: Kerry Emanuel (emanuel@mit.edu)

31   Abstract

32   Cyclonic storms resembling tropical cyclones are sometimes observed well outside the
33   tropics. These include medicanes, polar lows, subtropical cyclones, Kona storms, and
34   possibly some cases of Australian East Coast Lows. Their structural similarity to tropical
35   cyclones lies in their tight, nearly axisymmetric inner cores, eyes, and spiral bands.
36   Previous studies of these phenomena suggest that they are partly and sometimes
37   wholly driven by surface enthalpy fluxes, as with tropical cyclones. Here we show,
38   through a series of case studies, that many of these non-tropical cyclones have
39   morphologies and structures that resemble each other and also closely match those of
40   tropical transitioning cyclones, with the important distinction that the potential intensity
41   that supports them is not present in the pre-storm environment but rather is locally
42   generated in the course of their development. We therefore propose to call these storms
43   CYClones from Locally Originating Potential intensity (CYCLOPs). We emphasize that
44   mature CYCLOPs are essentially the same as tropical cyclones but their development
45   requires substantial modification of their thermodynamic environment on short time
46   scales. Like their tropical cousins, the rapid development and strong winds of CYCLOPs
47   pose a significant threat and forecast challenge for islands and coastal regions, and the
48   effects of climate change on them should be considered.

49

50   1.   Introduction

51   Cyclones that resemble tropical cyclones are occasionally observed to develop well outside the
52   tropics. These include polar lows, medicanes, subtropical cyclones, Kona storms (central North
53   Pacific), and perhaps some cases of Australian East Coast Lows. The identification of such
54   systems is usually based on their appearance in satellite imagery and on the environmental
55   conditions in which they occur. Here we show that many of these systems are manifestations of
56   the same physical phenomenon and, as such, should be given a common, physically-based
57   designation. We propose to call these CYClones from Locally Originating Potential intensity
58   (CYCLOPs), with reference to the one-eyed creatures of Greek mythology[1]. We show that in
59   many respects these developments resemble classical "tropical transition" (TT) events (e.g.
60   Bosart and Bartlo, 1991), but they are distinguished from the latter by occurring in regions
61   where the climatological potential intensity is small or zero. (Some events previously identified
62   as TT events were probably examples of CYCLOPs.) Their often-rapid development and

---

[1] Late in the process of writing this paper, we discovered that there is a scientific research project by the same name, standing for "Improving Mediterranean CYCLOnes Predictions in Seasonal forecasts with artificial intelligence" (https://www.cmcc.it/projects/CYCLOPs-improving-mediterranean-cyclones-predictions-in-seasonal-forecasts-with-artificial-intelligence). Its team leader, Leone Cavicchia, has graciously agreed with our use of the same name.

63   intense mesoscale inner cores, compared to extratropical cyclones, make CYCLOPs significant
64   hazards and a forecasting challenge.

65   Cyclones of synoptic and sub-synoptic scale are powered by one or both of two energy sources:
66   the available potential energy (APE) associated with isobaric temperature gradients
67   (baroclinity), and fluxes of enthalpy (sensible and latent heat) from the surface (usually the
68   ocean) to the atmosphere[2]. A normal extratropical cyclone over land is an example of the
69   former, while the latter is epitomized by a classical tropical cyclone. Extratropical transitioning
70   and tropical transitioning cyclones[3] can be ~~are~~ powered by both sources, either in sequence or
71   with the relative proportion ~~usually~~ varying over the life of the storm (see, e.g., Fantini, 1990).
72   Additionally, we note that tropical cyclones often originate in disturbances, such as African
73   easterly waves, that derive their energy from baroclinic and barotropic sources.

74   Like tropical cyclones, CYCLOPs are mainly powered by surface enthalpy fluxes, but differ from
75   the former in that the required potential intensity is produced locally and transiently, whereas
76   tropical cyclones develop in seasons and regions where sufficient potential intensity is always
77   present. CYCLOPs closely resemble the strongly baroclinic cases of tropical transition defined
78   and discussed by Davis and Bosart (2004), except that they occur in regions where the
79   climatological potential intensity is too small for tropical cyclogenesis, relying on synoptic-scale
80   perturbations that locally enhance potential intensity in space and time. Davis and Bosart (2004)
81   confined their attention to tropical cyclone formation in regions of high sea surface temperature,
82   stating that "The precursor cyclone must occlude and remain over warm water ($\gtrsim 26°C$) for at
83   least a day following occlusion." Similarly, McTaggart-Cowan et al. (2008) and McTaggart-
84   Cowan et al. (2013) only examined cases of tropical transition that resulted in named tropical
85   cyclones. But McTaggert-Cowan et al. (2015) recognized that around 5% of the cases they
86   identified as tropical transition cases occurred over colder water and that upper-level troughs
87   played a key role in destabilizing the atmosphere with respect to the sea surface. We here build
88   on this work and place it within the framework of potential intensity theory.

89   The basic physics of CYCLOPs was explored by the first author in reference to medicanes
90   (Emanuel, 2005), and is illustrated in Figure 1. While the actual evolution is, of course,
91   continuous, it is simpler to discuss it in phases. For this narrow purpose, we assume that a cut-
92   off cyclone has already formed in the upper troposphere, signified by the presence of an
93   isolated potential vorticity (PV) anomaly near the tropopause (Figure 1a). We show an idealized
94   circularly symmetric anomaly and a cross-section through it; in practice, such developments are
95   seldom close to axisymmetric in their earlier stages. In the illustration, the first phase is
96   assumed to occur over land, but that need not be the case in general.

---

[2] Some would regard latent heating as an additional energy source, but condensation through a deep layer is present in most cyclones and, being strongly tied to vertical motion, should not be regarded as an external heat source but rather as a modification of the static stability (Emanuel et al., 1994).

[3] Extratropical transitioning cyclones are storms whose energy source is transitioning from surface fluxes to ambient baroclinity, while the energy source of tropical transitioning cyclones is moving in the opposite direction.
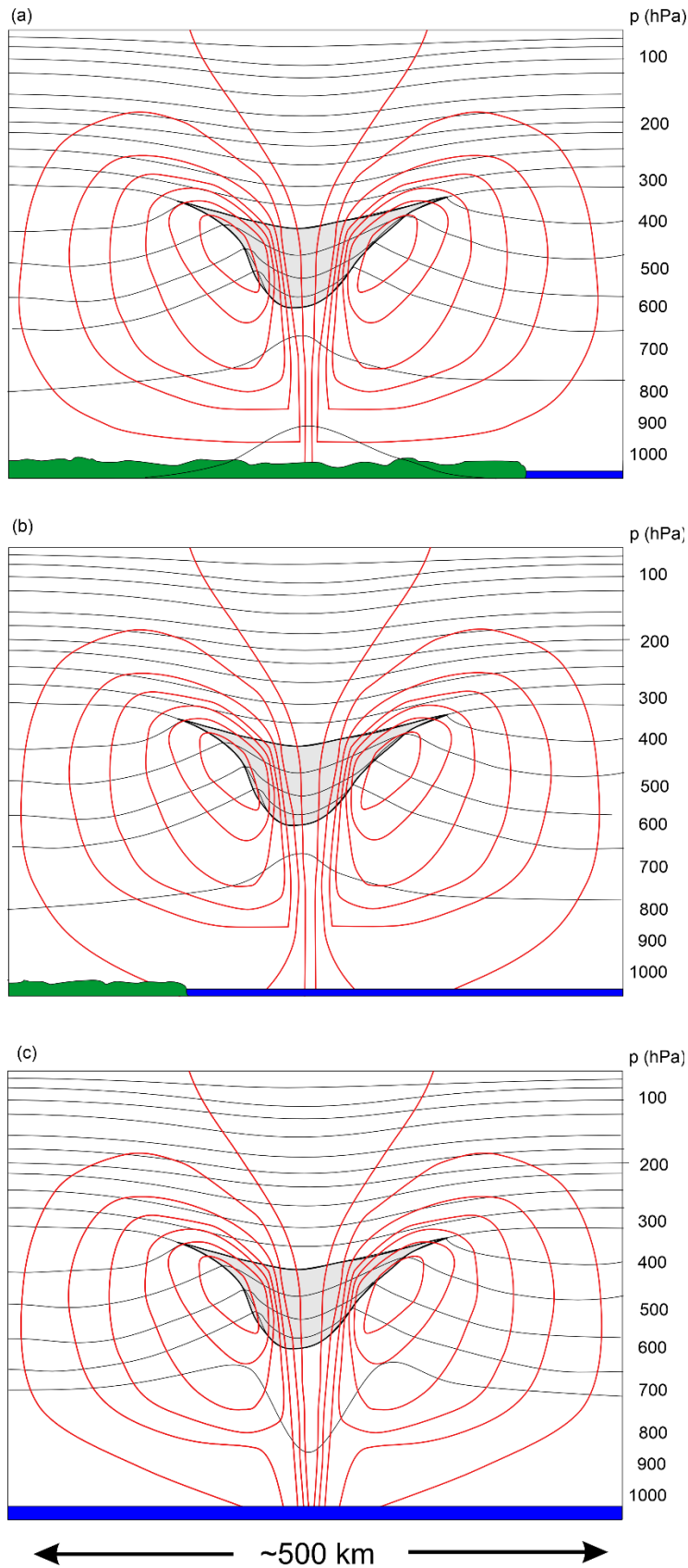
Figure 1: Three stages in the development of a CYCLOP. Each of the three panels shows a cross-section through an isolated PV anomaly at the tropopause (gray shading), idealized as circular. The thin black curves are isentropes, while the red curves are isotachs of the flow normal to the cross-section. In the first phase (a), the PV anomaly is over land, the troposphere beneath it is anomalously cold, and there may be no flow at the surface. The system moves out over open water in the next phase (b) and warming of the boundary layer and lower troposphere suffices to eliminate the cold anomaly at and near the surface. Weak cyclonic flow develops in response to the positive PV anomaly aloft. In the final phase (c), the surface heat fluxes become important and a tight, inner warm core develops.

~500 km

98   During the creation of the near-tropopause PV anomaly, some combination of lifting and cold air
99   seclusion has cooled and humidified the column underneath the PV anomaly, and the cold
100   anomaly extends right to the surface. From a PV inversion perspective, the near-surface
101   anticyclone that results from inverting the negative potential temperature anomaly at the surface
102   is assumed to just cancel the cyclonic anomaly that results from inverting the tropopause PV
103   anomaly, yielding no circulation at the surface. This assumption is made for simplicity here and
104   we do not mean to imply that such a cancellation is common.

105   In phase 2 (Figure 1b), the system drifts out over open water that is warm enough to diminish
106   and eventually eliminate the cold anomaly at the surface, "unshielding" it from the PV anomaly
107   aloft. During this phase, a cyclonic circulation develops in the lower troposphere, with a
108   horizontal scale commensurate with that of the PV anomaly.

109   If the local potential intensity is large enough, and the air aloft sufficiently close to saturation,
110   Wind-Induced Surface Heat Exchange (WISHE) can develop a tropical cyclone-like vortex
111   (phase 3, Figure 1c), with a warm inner core, eye and eyewall, and perhaps spiral bands. Note
112   that the inner core may be warm only with respect to the synoptic-scale cold anomaly
113   surrounding it, not necessarily with respect to the distant environment. At mid-levels, the
114   temperature anomaly may manifest as a small-scale warm anomaly surrounded by a synoptic-
115   scale cold anomaly.

116   In reality, these phases blend together into a continuum. Moreover, all three phases may (and
117   often do) occur over water. One practical challenge is calculating the potential intensity. This
118   should be calculated using the temperatures of the sea surface and the free troposphere under
119   the PV anomaly aloft, but before the troposphere has appreciably warmed from surface fluxes.
120   In practice, because the warming occurs either as the PV anomaly develops over water, or as it
121   moves over water from land, we have no access to the sounding of the free troposphere *before*
122   it has warmed up. The true potential intensity for a TC developing within the cold column under
123   the PV anomaly is hence impossible to obtain. Nevertheless, we can estimate how cold the
124   troposphere was before surface fluxes warmed it by using the surface pressure perturbation as
125   a proxy for the CYCLOPs-induced warming, and assuming that the troposphere has an
126   approximately moist adiabatic temperature profile[4]. and using the surface pressure perturbation
127   as a proxy for the CYCLOPs-induced warming. This is derived in the Appendix. The result is a
128   modified potential intensity, V_{pm}, given by

$$V_{pm}^2 = V_p^2 - \frac{C_k}{C_D}\frac{T_s}{T_{400}}\phi'_{950},\tag{1}$$

130   where V_p is the potential intensity calculated in the usual way (e.g. Bister and Emanuel, 2002)

131   from the local sea surface temperature and atmospheric sounding, ϕ'_{950} is the perturbation away

132   from climatology of the near-surface geopotential, which we here evaluate at 950 hPa, C_k and

----

[4] In regions of deep convection, lapse rates are usually observed to be close to moist adiabatic (Betts, 1986)

133   C_D are the surface exchange coefficients for enthalpy and drag, and T_s and T_{400} are the

134   absolute temperatures at the surface and 400 hPa. As explained in the Appendix, we

135   approximate the coefficient multiplying ϕ'_{950} in (1) by a constant value, 1.3, a reasonable estimate

136   of the mean value of the coefficient. Note that (1) is only valid in places where our assumption

137   that the lapse rate is moist adiabatic trough a deep layer is valid and deep moist convection

138   occurs. Also, in the early stages of development, the outflow level is likely to be lower and the

139   outflow temperature correspondingly higher, reducing the value of the coefficient multiplying ϕ'_{950}

140   in (1).

141   Beginning with an upper cold cyclone in an environment of otherwise zero potential intensity,

142   Emanuel (2005) simulated the development of a WISHE-driven cyclone using the axisymmetric,

143   nonhydrostatic hurricane model of Rotunno and Emanuel (1987). The cold, moist troposphere

144   under such an upper cyclone proves to be an ideal incubator of surface flux-driven cyclones

145   with characteristics nearly identical to those of tropical cyclones. One interesting facet of the

146   process is that the anomalous surface enthalpy flux destroys the parent upper cold low over a

147   period of a few days, through the action of deep convection. This in another way in which

148   CYCLOPs are distinguished from tropical cyclones, which tap spatially extensive regions of high

149   potential intensity.

150   2.   Why it matters

151   Why should we care whether a cyclone is driven by surface fluxes or baroclinity? From a

152   practical forecasting standpoint, the spatial distributions of weather hazards, like rain and wind,

153   can be very different, as can be the development time scales and fundamental predictability.

154   In classical baroclinic cyclones, the strongest winds are often found in frontal zones and can be

155   far from the cyclone center, while precipitation is usually heaviest in these frontal zones and in a

156   shield of slantwise ascent extending poleward from the surface cyclone. There is long

157   experience in forecasting baroclinic storms, and today's numerical weather prediction (NWP) of

158   these events has become quite accurate, even many days ahead. Importantly, baroclinic

159   cyclones are well resolved by today's NWP models. While baroclinic cyclones can intensify

160   rapidly, both the magnitude and timing of intensification are usually forecast accurately, and

161   uncertainties are well quantified by NWP ensembles (Leutbecher and Palmer, 2008).

162   By contrast, the physics of tropical cyclone intensification, involving a positive feedback between

163   surface winds and surface enthalpy fluxes, results in an intense, concentrated core with high

164   winds and heavy precipitation (which can be snow in the case of polar lows). The eyewalls of

165   surface flux-driven cyclones are strongly frontogenetical (Emanuel, 1997), further concentrating

166   wind and rain in an annulus of mesoscale dimensions. The intensity of surface flux-driven

167   cyclones can change very rapidly and often unpredictably, presenting a severe challenge to

168   forecasters. For example, Hurricane Otis of 2023 intensified from a tropical storm to a Category

169   5 hurricane in about 30 hours, devastating Acapulco, Mexico, with little warning from

170   forecasters. The small size of the core of high winds and heavy precipitation means that small

171   errors in the forecast position of the center of the storm can lead to large errors in local wind and

172 precipitation predictions. Surface flux-driven cyclones are too small to be well resolved by
173 today's global NWP models, and even if they were well resolved, fundamental predictability
174 studies show high levels of intrinsic unpredictability of rapid intensity changes (Zhang et al.,
175 2014).

176 The time and space scales of surface flux-driven cyclones are such that they couple strongly
177 with the ocean, producing near-inertial currents whose shear-driven turbulence mixes to the
178 surface generally (but not always) colder water from below the surface mixed layer. This has an
179 important (usually negative) feedback on the intensification of such cyclones. Accurate
180 numerical forecasting of surface flux-driven cyclones therefore requires an interactive ocean,
181 generally missing from today's NWP models because it is not very important for baroclinic
182 cyclones and because of the additional computational burden.

183 For these reasons, it matters (or should matter) to forecasters whether a particular development
184 is primarily driven by surface fluxes or by ambient baroclinity. The structural differences
185 described above are often detectable in satellite imagery; at the same time, such imagery is
186 sometimes misleading about the underlying physics. For example, classical baroclinic
187 development sometimes develops cloud-free eyes surrounded by convection through the warm
188 seclusion process, even over land, and yet may not have the intense annular concentration of
189 wind and rain characteristic of surface flux-driven cyclones (Tous and Romero, 2013).

190

191 # 3.   Case Studies

192 Armed with the conceptual CYCLOP model developed in Section 1 and modified potential
193 intensity given by (1), we now turn to case studies of the development of medicanes, polar lows,
194 a subtropical cyclone, and a Kona storm, showing that the dynamic and thermodynamic
195 pathways are similar. Specifically, each case developed after the formation of a deep, cold-core
196 cut-off cyclone in the upper troposphere that often resulted from a Rossby wave breaking event.
197 The lifting of the tropospheric air in response to the developing potential vorticity anomaly near
198 the tropopause created a deep, cold, and presumably humid column. The deep cold air over
199 bodies of relatively warmer water substantially elevates potential intensity, while its high relative
200 humidity discourages evaporatively driven convective downdrafts, which tamp down the needed
201 increase in boundary layer enthalpy. Low vertical wind shear near the core of the cutoff cyclone,
202 coupled with high potential intensity and humidity, provide an ideal embryo for tropical cyclone-
203 like development. The requirement for low vertical wind shear may prevent open troughs from
204 producing CYCLOPs, even if the potential intensity is elevated.

205 In what follows we focus on the cut-off cyclone evolution and the development of modified
206 potential intensity. In a particular case, we compare reanalysis column water vapor to that
207 estimated from satellite measurements. The differences between these are significant enough
208 to cast some doubt on the quality of reanalyzed water vapor associated with the small-scale
209 CYCLOP developments, thus we do not focus on water vapor even though it is known to be
210 important for intensification of tropical cyclones.

211   We also examined, but do not show here, several cases of Australian East Coast Lows
212   (Holland et al., 1987). Owing to the East Australian Current, the climatological potential intensity
213   is substantial off the southeast coast of Australia, and the CYCLOP developments we analyzed
214   behaved more like classical tropical transitions, with little or no role of the synoptic scale
215   dynamics in enhancing the existing potential intensity. We suspect that there may be other
216   cases in which the latter process was important, but did not conduct a search for such cases. It
217   is clear that in many of these cases surface heat fluxes were important in driving the cyclone
218   (Cavicchia et al., 2019). We also examined a small number of subtropical cyclones that
219   developed in the South Atlantic, but as with the Australian cases, they resembled classical
220   tropical transitions, though again we suspect there may be CYCLOP cases there as well.

221   As with tropical cyclones, there are variations on the theme of CYCLOPs, and we explore these
222   in the closing sections.

223   ### 3.1 Medicane Celeno of January, 1995

224   On average, 1.5 medicanes are observed annually in the Mediterranean (Cavicchia et al., 2014;
225   Nastos et al., 2018; Romero and Emanuel, 2013; Zhang et al., 2021) and, more rarely, similar
226   storms are observed over the Black Sea (Yarovaya et al., 2008). We begin with a system,
227   Medicane Celeno, that reached maturity on 16 January, 1995, shown in infrared satellite
228   imagery in Figure 2.

229
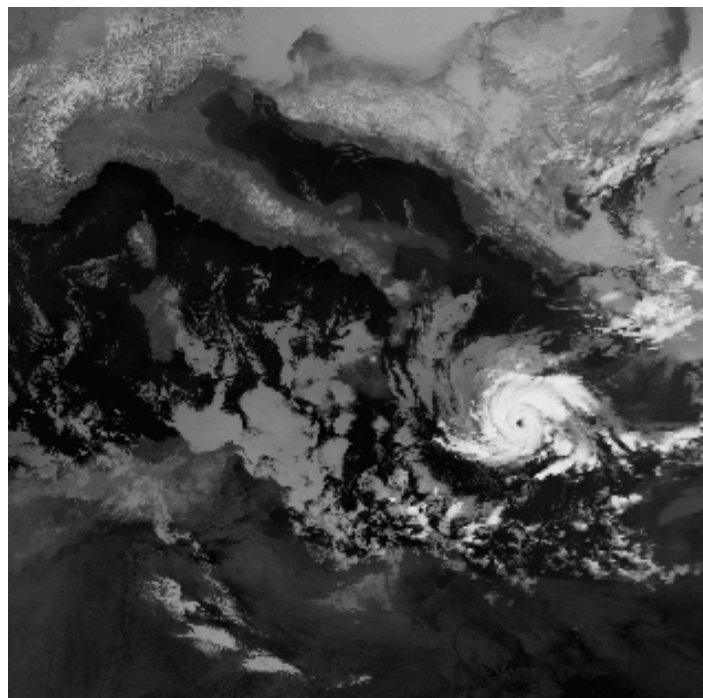
230   *Figure 2: Infrared satellite image of Medicane Celeno in the central Mediterranean, at 09:06 UTC 16 January 1995.*
231   *(Image credit: NOAA, 1995)*

232
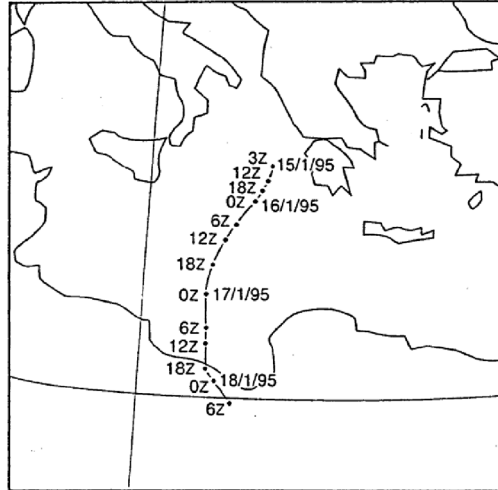
234 *Figure 3: Track of the surface center of the cyclone between 03:00 UTC on January 15 and 06:00 on January 18,*
235 *1995, derived from satellite images (Pytharoulis et al.,1999)*

236 Figure 3 shows the track of the surface center of the cyclone, which developed between Greece
237 and Sicily and made landfall in Libya. A detailed description of this medicane is provided by
238 Pytharoulis et al. (1999).

239 The evolution of the system in increments of 24 hours, beginning on 00 UTC, 12 January and
240 ending at 00 UTC 15 January, is shown in Figure 4. This sequence, showing the 400 hPa and
241 950 hPa geopotential heights, covers the period leading up to the CYCLOP development. The
242 evolution of the upper tropospheric (400 hPa) height field shows a classic Rossby wave
243 breaking event (McIntyre and Palmer, 1983) in which an eastward-moving baroclinic Rossby
244 wave at higher latitudes amplifies and irreversibly breaks to the south and west, finally forming a
245 cut-off cyclone. It is important to note that the formation of a cut-off cyclone in the upper
246 troposphere involves a local conversion from kinetic to potential energy, with deep cooling
247 associated with dynamically forced ascent (Gan and Piva, 2016). To the southeast of this
248 trough, a weak, broad area of low geopotential height develops at 950 hPa mostly over land in a
249 region of low-level warm advection. As the cold air under the cut-off low is gradually heated by
250 the underlying sea, a broad surface cyclone develops by 00 UTC on January 14th. At around
251 this time, the feedback between surface wind and surface enthalpy fluxes is strong enough to
252 develop a tight inner warm core (warm, that is, relative to the surrounding cold pool, not
253 necessarily to the unperturbed larger scale environment) and by 00 UTC on January 15th, it is
254 noticeable just to the west of northwestern Greece (Figure 5d). At the same time, the upper cold
255 core weakens, perhaps aided by the strong heating from the surface transferred aloft by deep
256 convection.

257
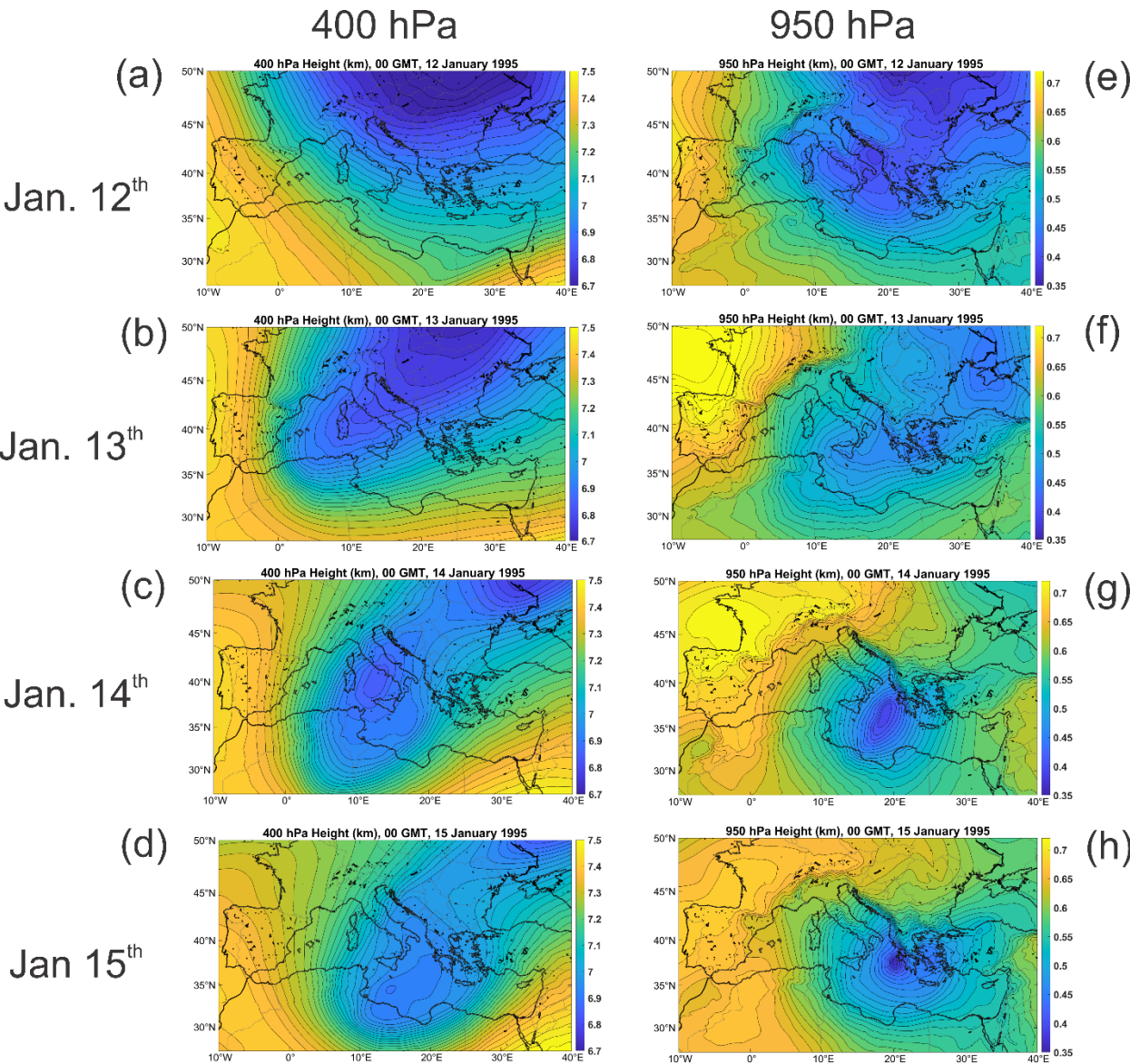
Figure 4: Evolution of the 400 hPa (left) and 950 hPa (right) geopotential heights in 24-hour increments, from 00 UTC 12 January to 00 UTC 15 January, 1995. These fields are from ERA5 reanalysis. The 400 hPa heights span from 6.7 to 7.5 km at increments of 26.67 m, while the 950 hPa heights range from 350 m to 730 m at increments of 12.67 m.

258

259
260
261
262

263

750 hPa T (K)   Modified Potential Intensity (m/s)
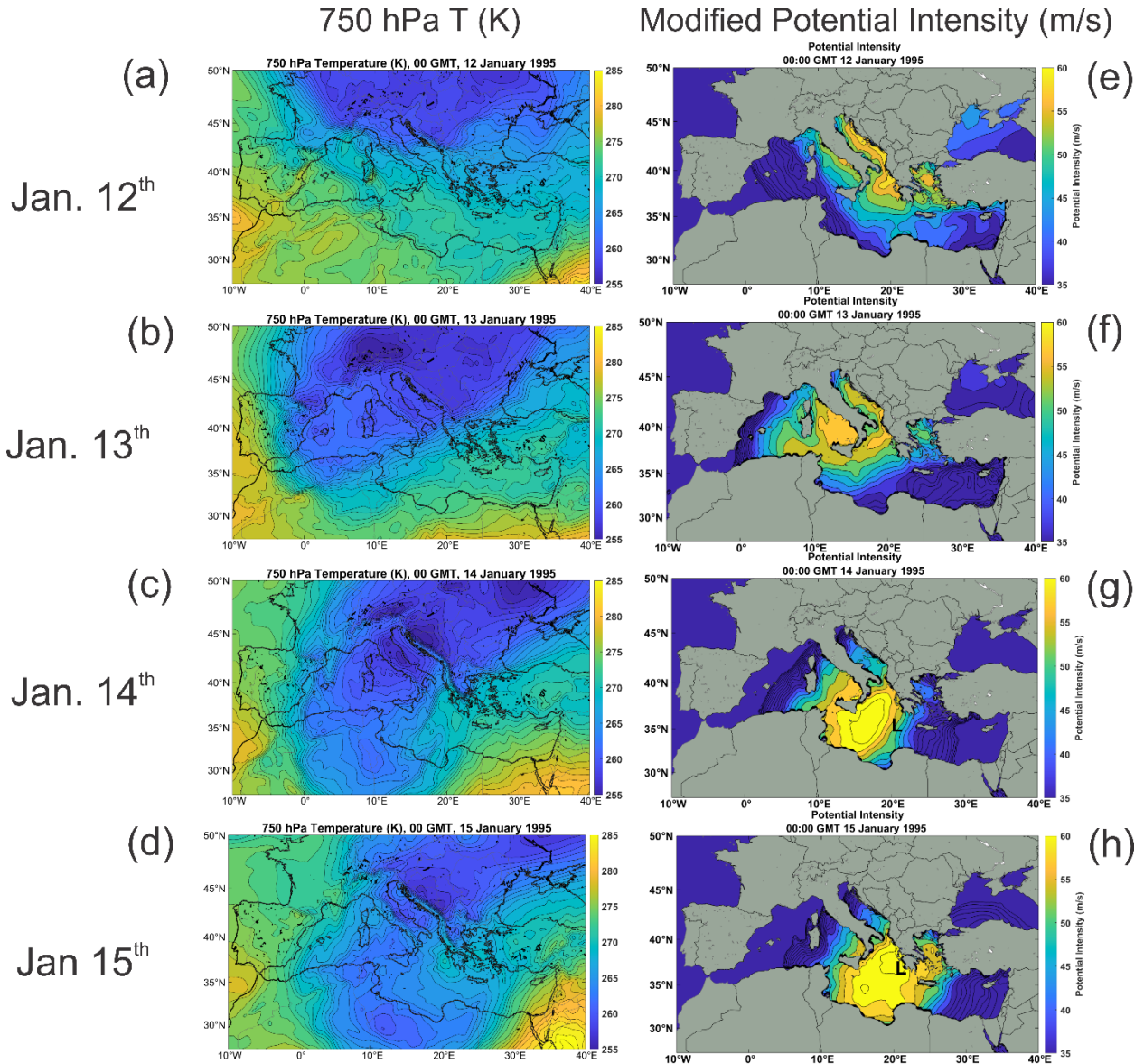
Figure 5: 750 hPa temperature (K; left) and modified potential intensity given by equation (1) (m/s, right) at 00 UTC on January 12th – 15th (top to bottom) 1995. The 750 hPa temperature spans from 255 K to 285 K at increments of 1 K, while the modified potential intensity ranges from 35 to 60 ms^{-1}at increments of 4 ms^{-1}. The black "L"s in panels g) and h) show the positions of the surface cyclone. From ERA5 reanalysis.

Figure 5 shows the corresponding evolution of the 750 hPa temperature and the modified potential intensity, V_{pm}, given by (1). The latter is only shown in the range of $35\,ms^{-1}$ to $60\,ms^{-1}$. Experience shows that tropical cyclone genesis is rare when the potential intensity is less than about $35\,ms^{-1}$ (Emanuel, 2010).

273   On January 12th, relatively small values of V_{pm} are evident in the eastern and northern

274   Mediterranean, but with higher values developing over the northern Adriatic as cold air aloft

275   creeps in from the north. As the upper tropospheric Rossby wave breaks and a cut-off cyclone

276   develops over the central Mediterranean, V_{pm} increases greatly during the 13th and 14th, with

277   peak values greater than $60\ ms^{-1}$. The CYCLOP develops in a region of high V_{pm}, though not

278   where the highest values occur, until the 15th at which time the mature CYCLOP location

279   corresponds to that of the highest V_{pm}. Note that a lower warm core is not obvious at 750 hPa

280   until January 15th and that it occurs on a somewhat smaller scale than the cut-off cyclone.

281   Figure A1 of the Appendix shows the individual contributions, on January 14th and 15th, of the

282   usual potential intensity (first term on the right side of (1)) and the correction for column warming

283   (second term on right of (1)) to the full potential intensity. (The contribution of column warming

284   was negligible before the 14th.) Note that the full potential intensity shown in Figure 5 *g* and *h* is

285   not the arithmetic sum of the two contributions but rather their Euclidean norm. The contribution

286   of the column warming, as measured by the surface pressure anomaly, is quite localized around

287   the CYCLOP and is located eastward of the maximum of the usual potential intensity.

288   As the CYCLOP moves southward, it maintains a tight inner warm core until after landfall (not

289   shown here) and the modified potential intensity, V_{pm}, over the south-central Mediterranean

290   diminishes rapidly, with peak values of only about $50\ ms^{-1}$ by 00 UTC on January 16th. One

291   potentially important difference between CYCLOP development and tropical transition is that in

292   the former case, the volume of air with appreciable potential intensity is limited. It is possible

293   that, by warming the whole tropospheric column relative to the surface, the enhanced surface

294   fluxes associated with the CYCLOP, acting through deep convection, substantially diminish the

295   magnitude and/or volume of the high V_{pm} air, serving to limit the lifetime of the CYCLOP. This

296   was the case in the axisymmetric numerical simulations of Emanuel (2005).

297   It is clear that this CYCLOP development occurred on time and space scales appreciably

298   smaller than those of the rather weak, synoptic-scale cyclogenesis resulting from the interaction

299   of the positive PV perturbation near the tropopause with a low-level temperature gradient. It is

300   also clear that the strong cooling of the troposphere in response to the development and

301   southward migration of the cutoff cyclone aloft was instrumental in bringing about the high

302   potential intensity necessary to activate the WISHE process. Therefore, the Rossby wave

303   breaking did much more than trigger cyclogenesis; it provided the necessary potential intensity

304   for the CYCLOP development. Here we draw a distinction from tropical transition, in which, in

305   most cases, the pre-existing potential intensity suffices to maintain a surface flux-driven cyclone.

306   We emphasize again that there is a gray area here consisting of flux-driven cyclones in which

307   the existing reservoir of potential intensity is enhanced to some degree by the local synoptic-

308   scale dynamics.

309

310

3.2 Medicane of December 2005

312   A medicane, unofficially known as Zeo, formed on December 14th 2005 off the coast of Tunisia
313   and then moved eastward across a large stretch of the Mediterranean. Figure 6 shows a
314   satellite image of this medicane on December 15th. This cyclone has been the subject of
315   several intensive studies (e.g. Fita and Flaounas, 2018; Miglietta and Rotunno, 2019).

316
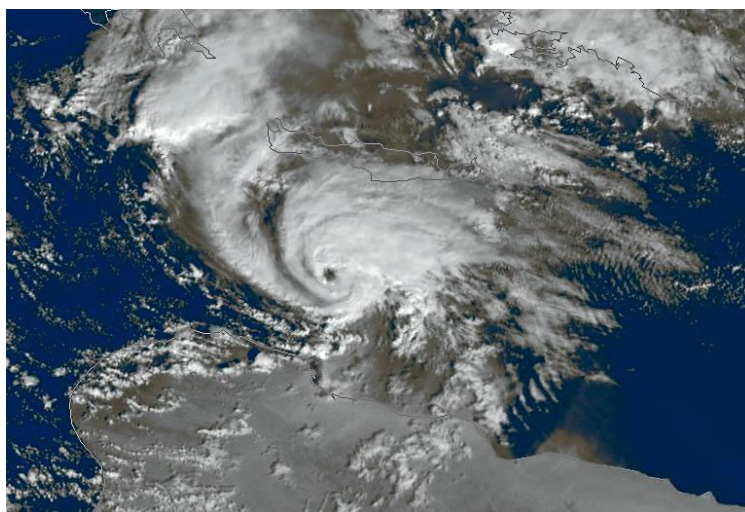
317   *Figure 6: Medicane Zeo between Crete and Libya on 15 December 2005. Image from NASA.*

318   Like Medicane Celeno, Medicane Zeo formed as a result of a Rossby wave breaking event, as
319   illustrated in Figure 7. On December 8th (panel a), a deep trough is digging southward over
320   eastern Europe, but by the 9th (panel b) it has split in two, with the westward half breaking
321   southwestward over Germany and Switzerland. By the 11th (panel d), this local minimum is
322   located over Tunisia and on the 12th (panel e) it is more or less completely cut off from the main
323   westerly jet. It subsequently oscillates over Tunisia and Algeria, before moving slowly eastward
324   over the Mediterranean, as shown in Figure 8.

325   In response to the cutoff cyclone development, a broad, synoptic-scale surface cyclone formed
326   to the east of the upper cyclone over the deserts of Libya during December 12th and 13th (not
327   shown here). The poorly defined center of this system drifted northward, on collision course with
328   the upper cyclone, which was drifting eastward over Tunisia by late on the 13th. As the surface
329   center moved out over the Mediterranean early on the 13th, rapid development ensued and a
330   mature CYCLOP was evident by 00 UTC on the 14th (Figure 8c). The system began to move
331   eastward and reached peak intensity on the 14th (left panels of Figure 8). The CYCLOP moved
332   eastward, along with its parent upper cyclone, and dissipated in the far eastern Mediterranean
333   on the 16th (not shown).

334

335

336
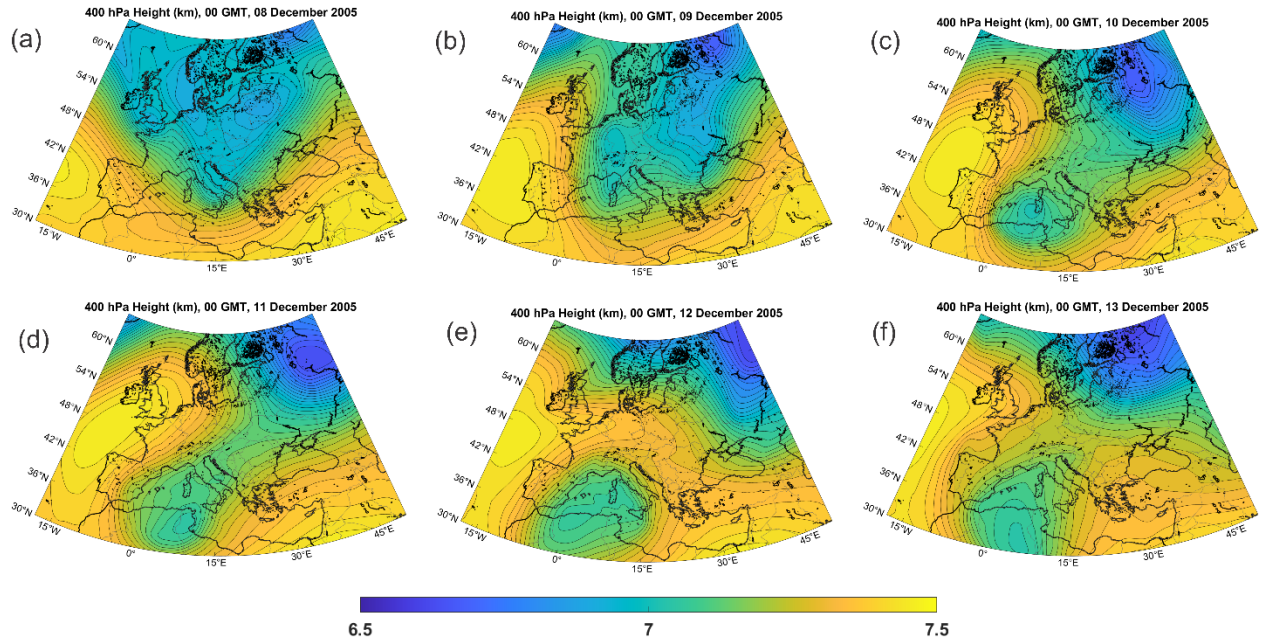
Figure 7: 400 hPa geopotential heights, ranging from 6.5 km to 7.5 km (color scale identical for all panels) at 00 UTC on December 8th (a), 9th (b), 10th (c), 11th (d), 12th (e), and 13th (f), 2005. From ERA-5 reanalysis. Contour interval is 33.3 m.

340   The evolutions of 750 hPa temperature and V_{pm} on the 14th and 15th of December are shown in

341   Figure 9. In this case, there were large meridional gradients of sea surface temperature across

342   the Mediterranean, ranging from over 20°C in the far south to less than 12°C in the northern

343   reaches of the Adriatic and western Mediterranean (not shown here). As the cold pool moved

344   southwestward and deepened, only low values of V_{pm} are present over the Mediterranean, but

345   beginning on December 10th, higher values developed over the Gulf of Sidra, east of Tunisia,

346   and by the 14th (Figure 9c) had reached at least 80 ms^{-1}, enabling the formation of the CYCLOP.

347   As in the Celeno case, V_{pm} values diminish thereafter, possibly because of the warming of the

348   column by the surface enthalpy flux.

349

350
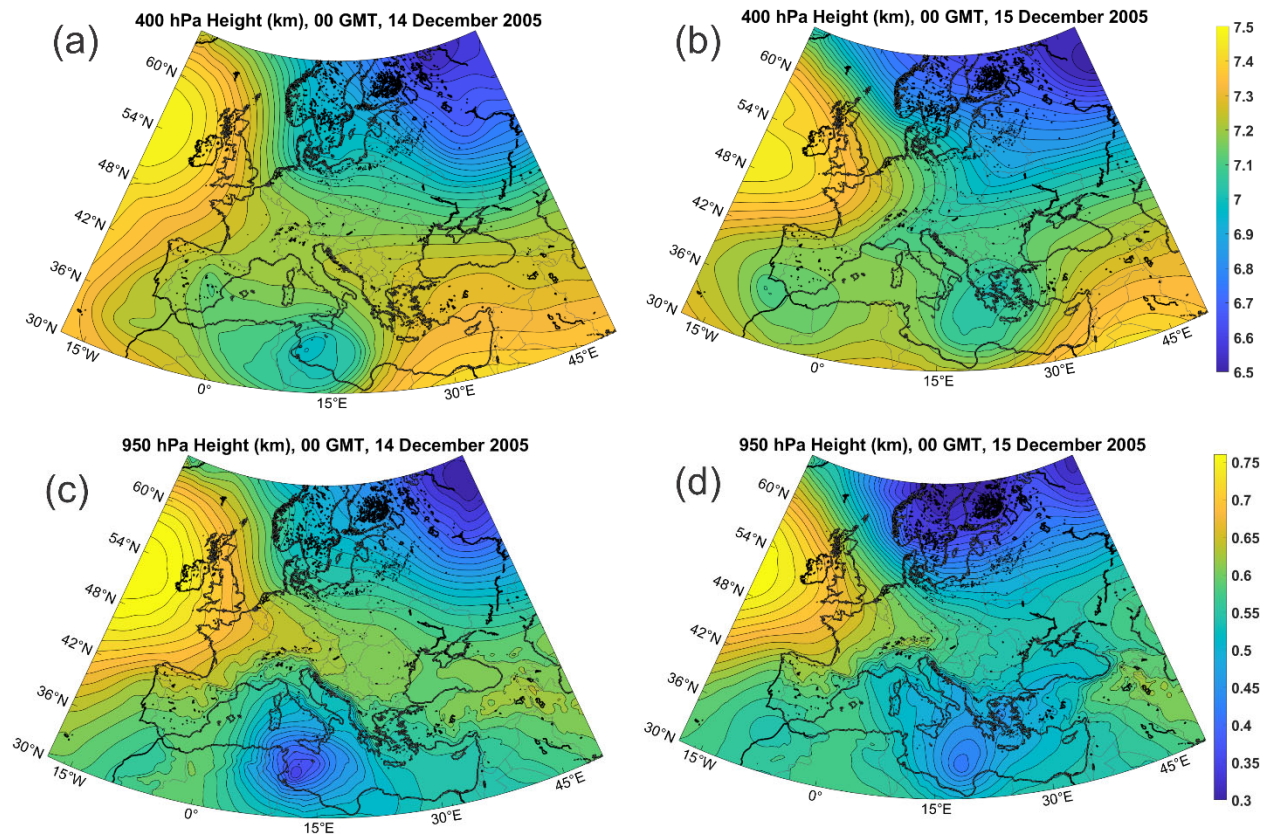
351 *Figure 8: Evolution of 400 hPa geopotential height, ranging from 6.5 to 7.5 km at contour interval of 36.7 m (a and b),*
352 *and 950 hPa geopotential height, ranging from 250 to 750 m at contour interval of 16.67 m (c and d) at 00 UTC in*
353 *December 14th (left) and 15th (right), 2005. The color scales of (a) and (b) are identical, as are the color scales of (c)*
354 *and (d). From ERA-5 reanalysis.*

355

356

358
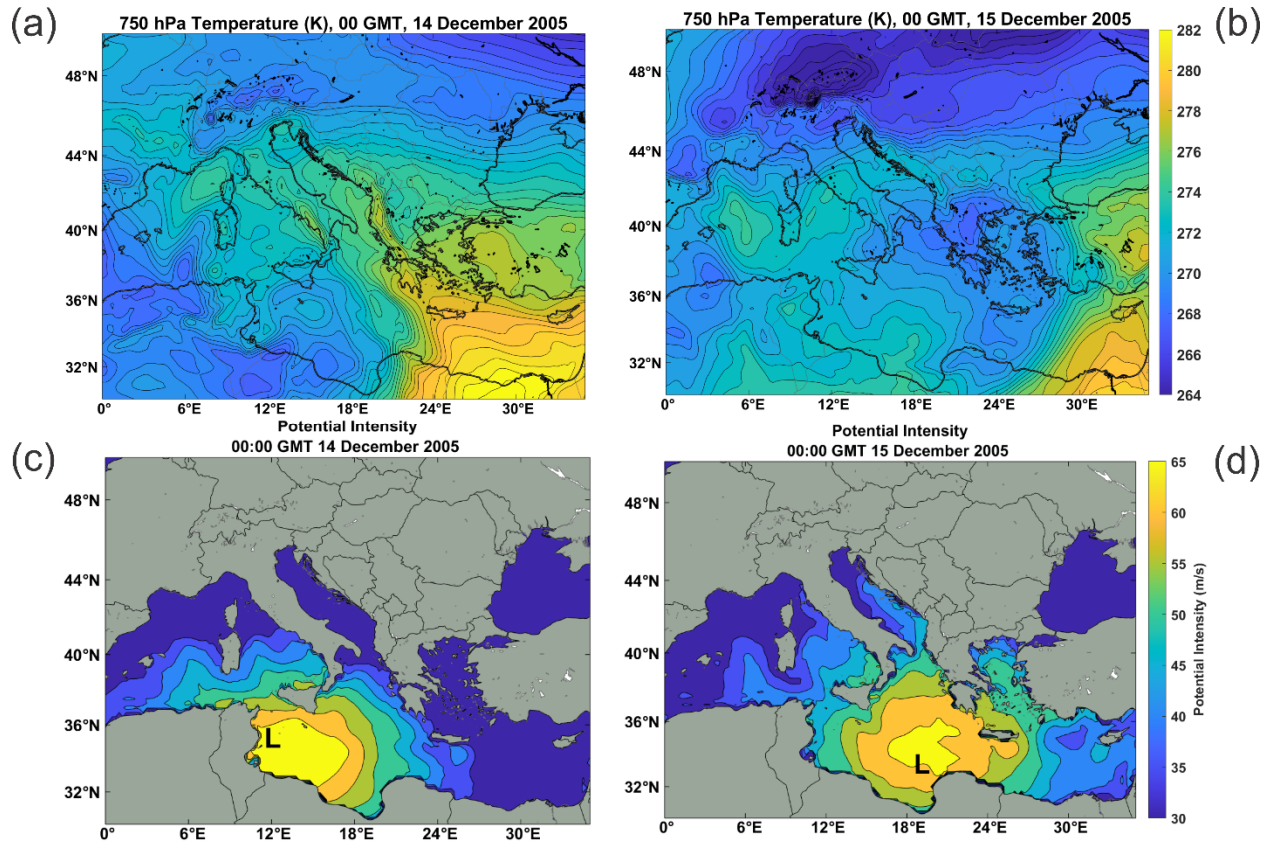
Figure 9: 750 hPa temperature at increments of 0.6 K (a-b) and modified potential intensity from 35 m s^{-1} to 65 m s^{-1} at increments of 5 m s^{-1} (c-d) at 00 UTC on December 14th (a,c) and December 15th (b,d) 2005. From ERA-5 reanalyses. The "L"s in c) and d) indicate the position of the 950 hPa cyclone center.

The 750 hPa temperature field (Figure 9a) shows a complex pattern of positive temperature perturbation near the position of the surface low, not nearly as focused as in the case of Medicane Celeno. As suggested by Fita and Flaounas (2018), part of the positive temperature anomaly associated with the cyclone may have resulted from a warm seclusion. Yet 24 hours later (Figure 9b) the warm anomaly near the cyclone center over the eastern Gulf of Sidra appears to have been advected from the south rather than the north. It is possible that the reanalysis did not capture the full physics of this particular medicane.

Figure 10 compares total column water retrieved from satellite microwave and near-infrared imagers (a) to that from the ERA5 reanalysis (b). While there is some broad agreement between the two estimates, the ERA5 underestimates column water in the critical region just east of Tunisia and overestimates it in an arc extending from eastern Sicily southeastward to the Libyan coast. Cyclop intensity, in analogy to tropical cyclone intensity, should be highly sensitive to low- and mid-level moisture in the mesoscale inner core region, which may be under-resolved and otherwise not well simulated by global NWP models. For this reason, we do not routinely show reanalysis of water vapor in this paper. The limitations of analyzed and forecast water vapor

377 may constitute an important constraint on CYCLOP predictability and is a worthy subject for
378 future research.
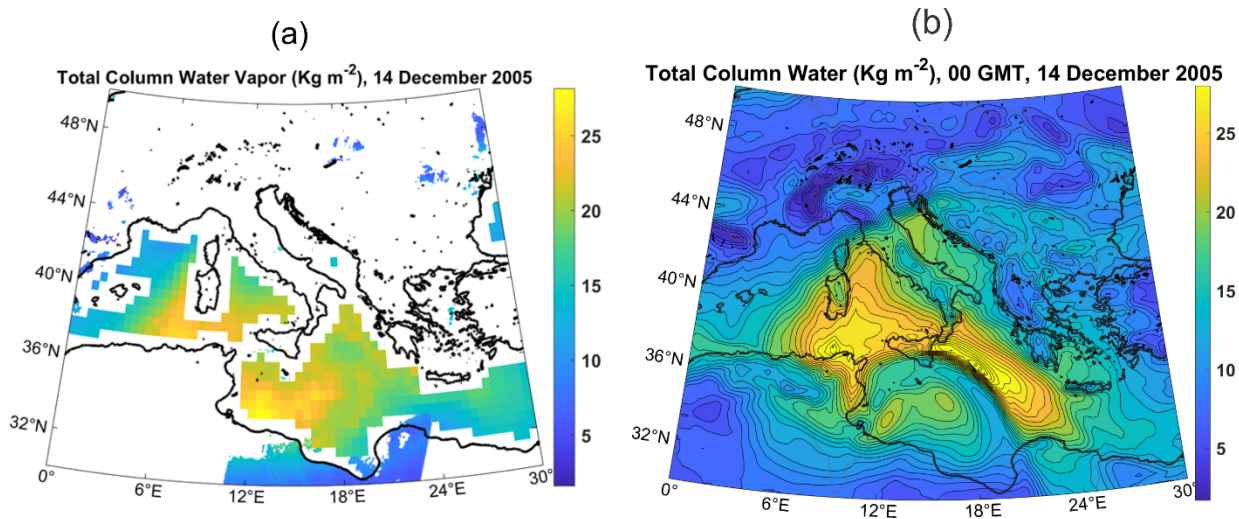
380 *Figure 10: Total column water vapor (Kg m⁻²) at 00 UTC on 14 December 2005, derived from microwave and near*
381 *infrared imagers (a) and ERA5 reanalysis (b). In (b) the contour increment is 0.9 Kg m⁻².*

3.3 Polar low of February, 1987

384 Closed upper tropospheric lows also provide favorable environments for CYCLOP development
385 at very high latitudes in locations where there is open water. These usually form poleward of the
386 mid-latitude jet, where quasi-balanced dynamics can be quite different from those operating at
387 lower latitudes. Figure 11 is an infrared image of a polar low that formed just south of Svalbard
388 on February 25th, 1987, and tracked southward, making landfall on the north coast of Norway on
389 the 27th. This system was studied extensively by Nordeng and Rasmussen (1992).

390
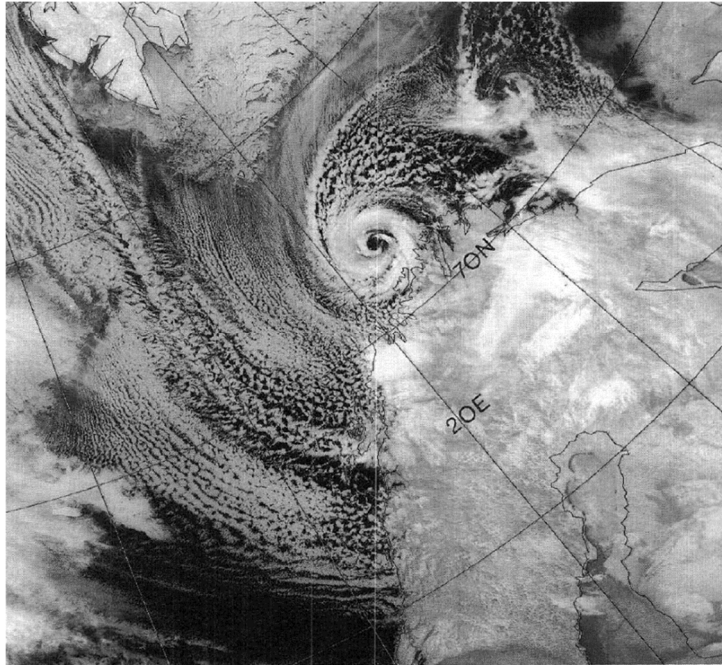
Figure 11: NOAA 9 satellite infrared image (channel 4) of a polar low just north of Norway at 08:31 UTC on 27 February 1987.

As with some medicanes, polar lows develop in strongly convecting air masses when cold air moves out over relatively warm water. The adjective "relatively" is crucial here; with polar lows the sea surface temperature is often only marginally above the freezing point of saltwater. Figure 12 shows the distribution of sea surface temperature on February 25th, with the uniform dark blue areas denoting regions of sea ice cover. The polar low shown in Figure 11 develops when deep cold air moves southward over open water, as shown in Figure 13.

In this case, it is not clear whether one can describe what happens in the upper troposphere (top row of Figure 13) as a Rossby wave breaking event. Instead, what we see is a complex rearrangement of the tropospheric winter polar vortex, as a ridge building over North America breaks and forms an anticyclone over the North Pole. This complex rearrangement results in the formation of a deep cutoff low just south of Svalbard by the 26th, which then moves southward over Norway by the 27th. The polar low is barely visible in the 950 hPa height field on the 25th (middle row of Figure 13), but intensifies rapidly as it moves over progressively warmer water, reaching maturity before landfall on the 27th.

407
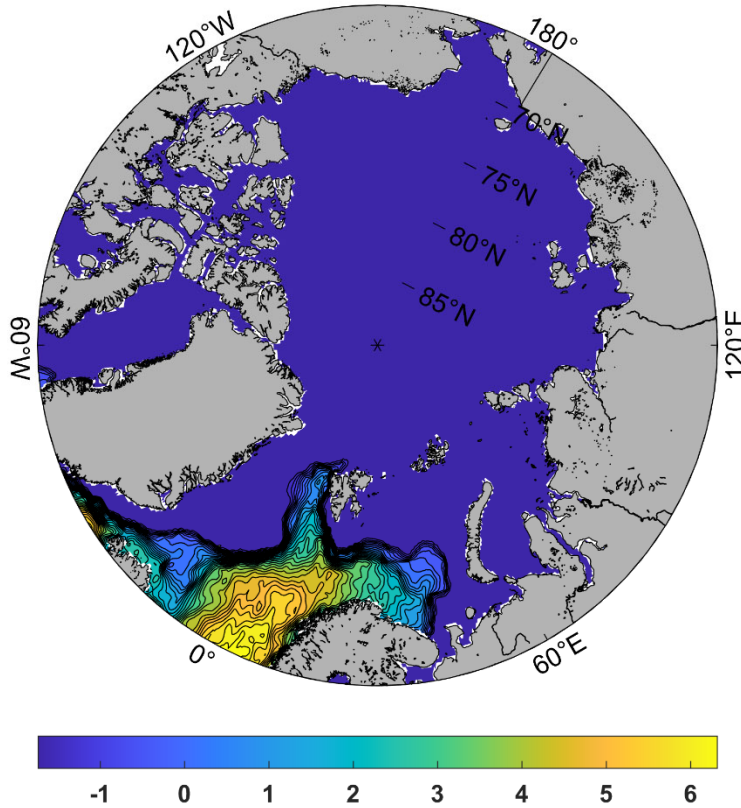
Figure 12: Sea surface temperature (ºC) in intervals of 0.3ºC at 02:00 UTC on 25 February, 1987, from ERA5 reanalysis. Dark blue areas denote regions of sea ice. From ERA-5 reanalyses.

408

409
410

411 The evolution of the V_{pm} field is shown in the bottom row of Figure 13. The potential intensity

412 increases rapidly south of Svalbard as the cut-off cyclone moves out over open water. (The

413 secondary region of high potential intensity, poleward of Siberia, is owing to relatively high ice

414 surface temperature in a region covered with sea ice. As there is very little heat flux through sea

415 ice, a CYCLOP cannot develop in this region, but a weak and broad surface low is associated

416 with the cutoff cyclone in the upper troposphere.)

417 Under these conditions, most of the surface flux that drives the CYCLOP is in the form of

418 sensible, rather than latent heat flux, and the background state has a nearly dry (rather than

419 moist) adiabatic lapse rate. As shown by Cronin and Chavas (2019) and Velez-Pardo and

420 Cronin (2023), surface flux-driven cyclones can develop in perfectly dry convecting

421 environments, though they generally reach smaller fractions of their potential intensity and lack

422 the long tail of the radial profile of azimuthal winds that is a consequence of the dry stratification

423 resulting from background moist convection (Chavas and Emanuel, 2014). They also have

424 larger eyes relative to their overall diameters. Given the low temperatures at which they occur,

425 polar lows may be as close to the Cronin-Chavas dry limit as one might expect to see in Earth's

426 climate.

427
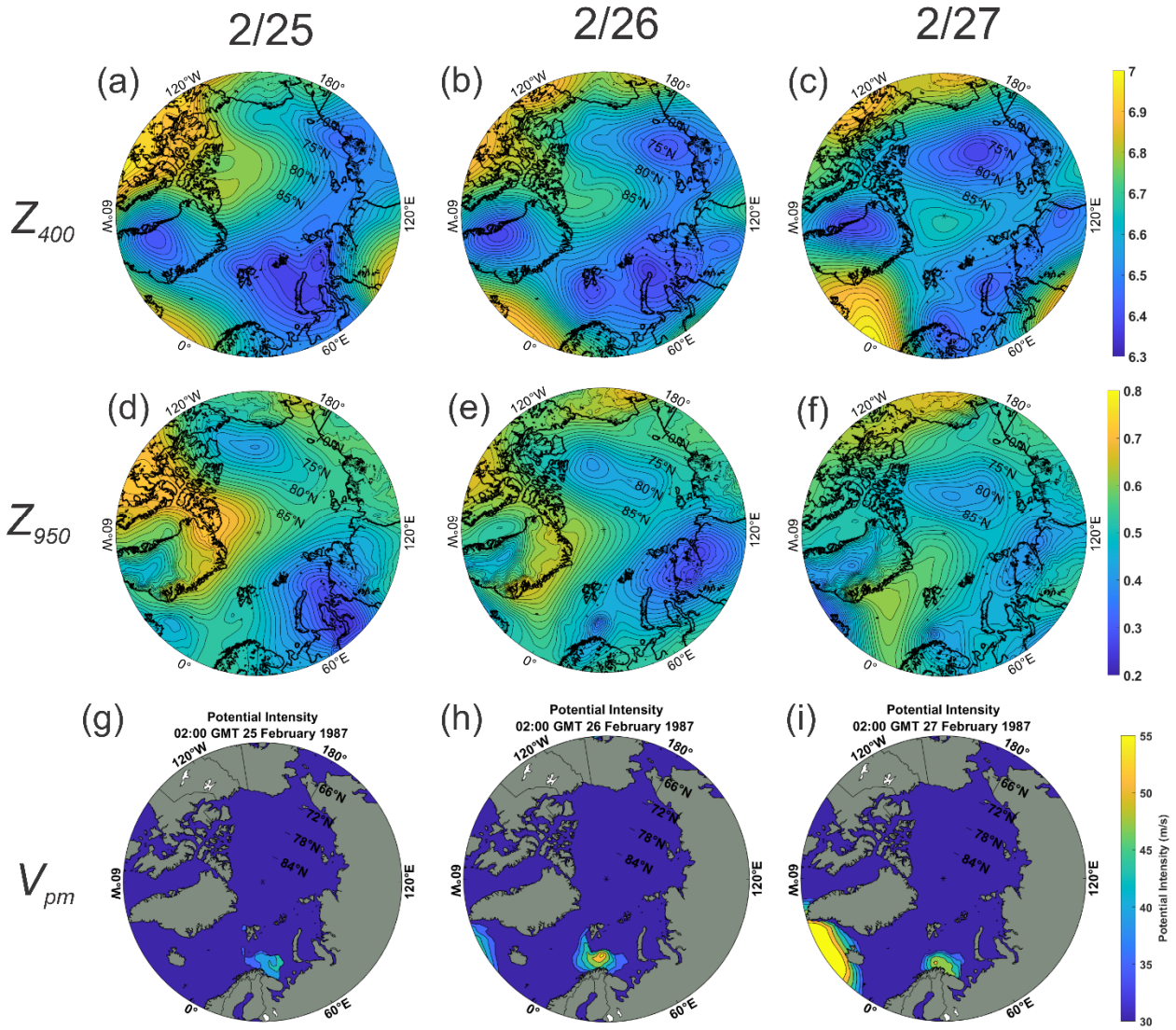
Figure 13: 400 hPa geopotential height (km)t at intervals of 23.3 m (a-c), 950 hPa geopotential height (km) in intervals of 20 m (d-f), and V_{pm} (ms^{-1}) in intervals of 4 ms^{-1} (g-i), at 02:00 UTC on February 25th (left), 26th (center), and 27th (right), 1987. From ERA-5 reanalysis.

One interesting feature of polar waters in winter is that the thermal stratification is sometimes reversed from normal, with warmer waters lying beneath cold surface waters. This is made possible, in part, by strong salinity stratification, that keeps the cold water from mixing with the warmer waters below. Therefore, it is possible for polar lows to generate warm, rather than cold, wakes, and this would feed back positively on their intensity. This seems to happen in roughly half the documented cases of polar lows in the Nordic seas (Tomita and Tanaka, 2024).

437 ## 3.4   Polar low over the Sea of Japan, December, 2009

438 Polar lows are not uncommon in the Sea of Japan, forming when deep, cold air masses from
439 Eurasia flow out over the relatively warm ocean. They are frequent enough to warrant a
440 climatology (Yanase and co-authors, 2016). A satellite image of one such storm is shown in
441 Figure 14.

442
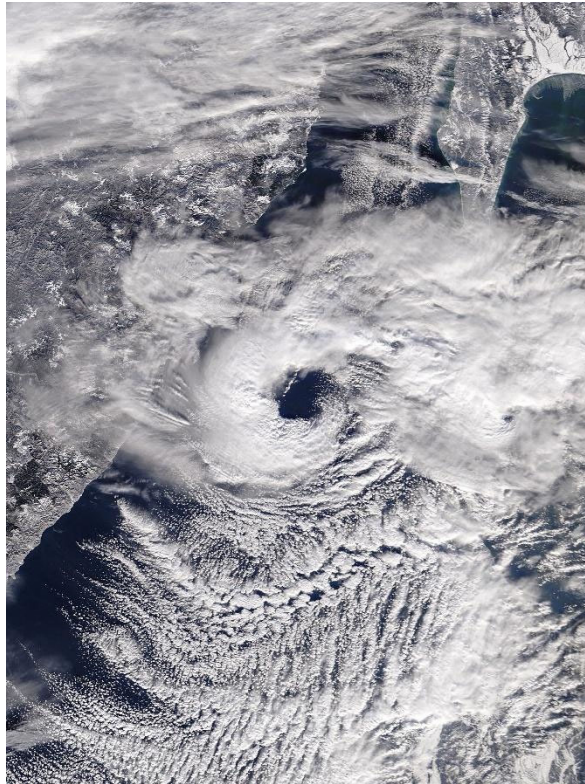
443 *Figure 14: Polar low over the northern Sea of Japan, 02:13 UTC 20 December, 2009 as captured by the MODIS*
444 *imager on NASA's Terra satellite.*

445 The cyclone traveled almost due south from this point, striking the Hokkaido region of Japan,
446 near Sapporo, with gale-force winds and heavy snow. As with other CYCLOPs, it formed in an
447 environment of deep convection under a cold low aloft.

448 The development of the cutoff cyclone aloft was complex, as shown by the sequence of 400
449 hPa maps displayed in Figure 15. These are 00 UTC charts at 1-day intervals beginning on
450 December 11th and ending on the 20th, about the time of the image in Figure 14. A large polar
451 vortex is centered in northern central Russia on the 11th but sheds a child low southeastward on
452 the 12th and 13th, becoming almost completely cutoff on the 14th. The parent low drifts westward
453 during this time. The newly formed cutoff cyclone meanders around in isolation from the 15th
454 through the 17th, but becomes wrapped up with a system propagating into the domain from the
455 east on the 18th. By the 20th, a small-scale cutoff cyclone is drifting southward over the northern
456 Sea of Japan, and it is this upper cutoff that spawns the polar low.

457
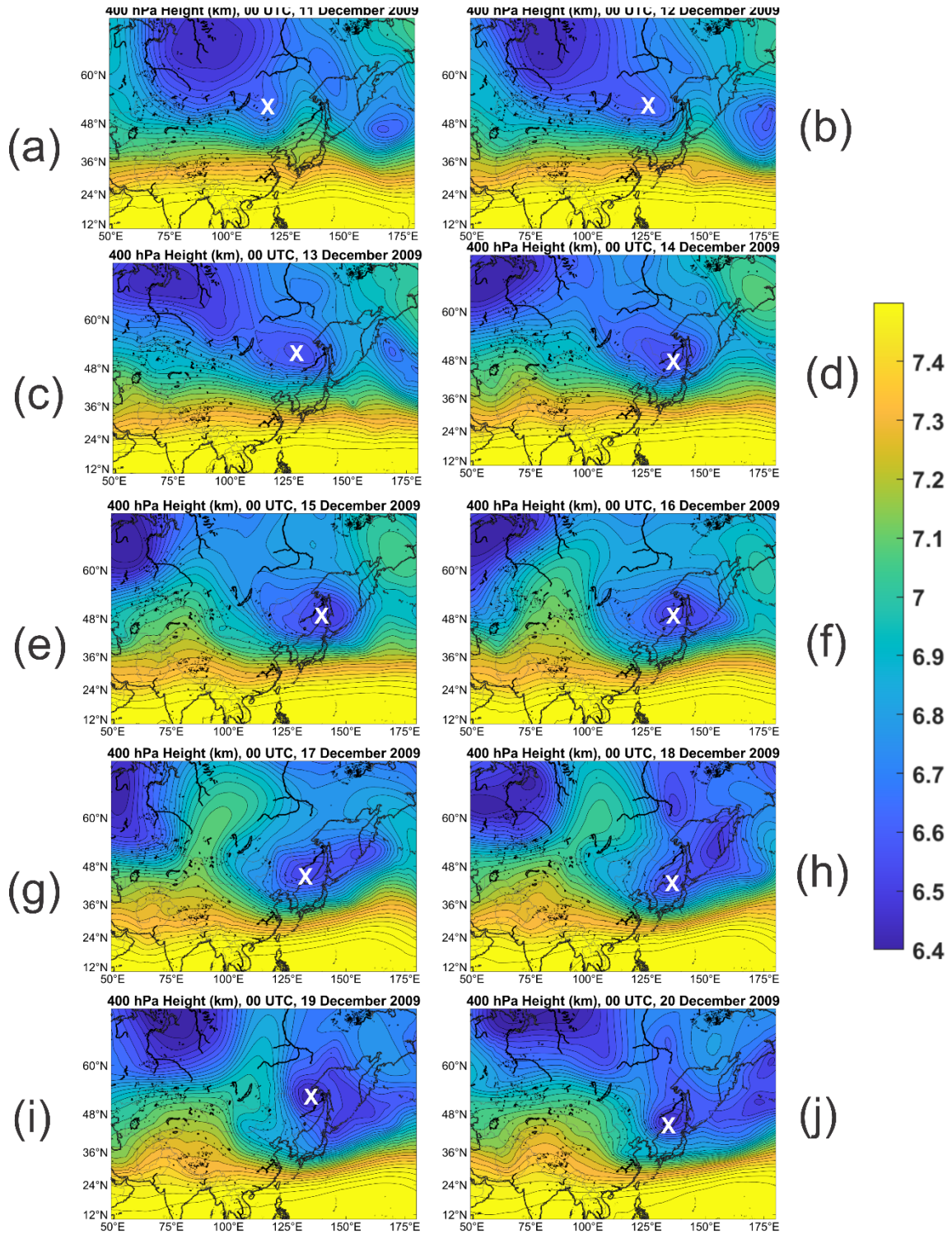
Figure 15: Sequence of 400 hPa geopotential height (km) charts at 1-day intervals from 00 UTC on December 11th (a) to 00 UTC on December 20th (j), 2009. The charts span from 0º to 180º longitude and from 10º to 70º latitude, and the contour increment is 36.7 m. The white crosses mark the center of the 400 hPa cyclone that was ultimately associated with the polar low. From ERA-5 reanalysis.

462   The 950 hPa height and the V_{pm} fields at 00 UTC on December 20th are shown in Figure 16. At
463   this time, the surface low is developing rapidly and moving southward into a region of high
464   potential intensity. The latter reaches a maximum near the northwest coast of Japan, where the
465   sea surface temperatures are larger. As with the two medicane cases and the other polar low
466   case, the CYCLOP develops in a place where the potential intensity values are normally too low
467   for surface flux-driven cyclones but for which the required potential intensity is created by the
468   movement of a deep cold cyclone aloft over relatively warm water. The reanalysis 750 hPa
469   temperature (not shown) presents a local maximum at the location of the surface cyclone at this
470   time.

(a)   (b)
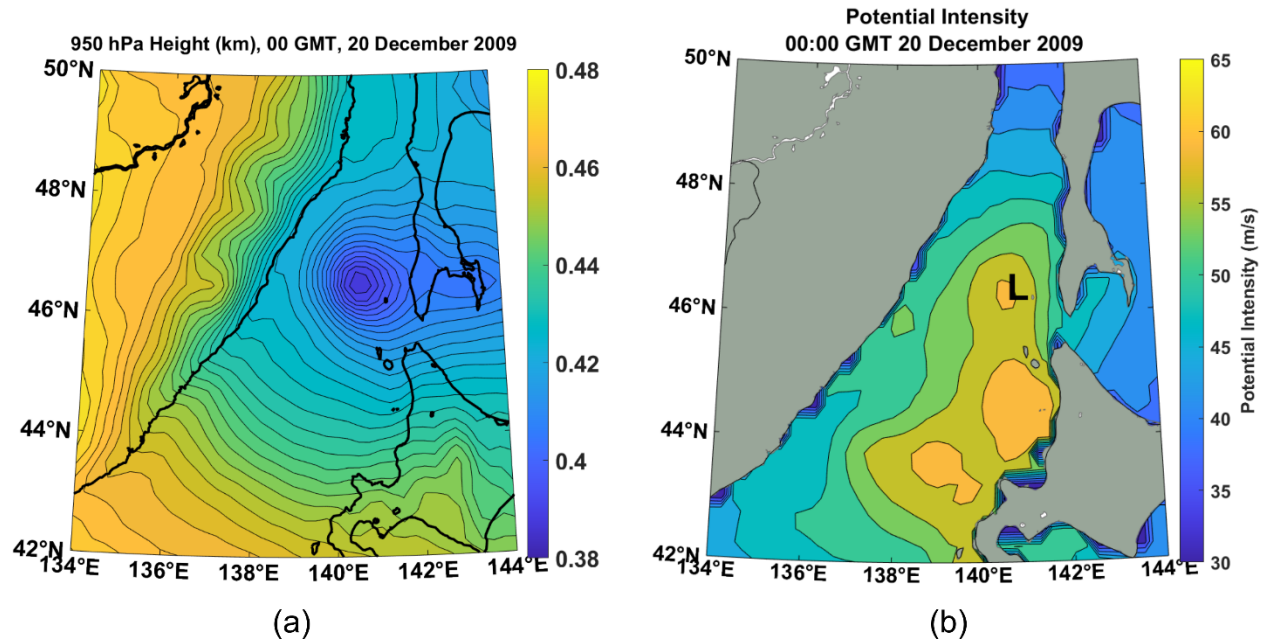
472   *Figure 16: 950 hPa geopotential height (a; km) at intervals of 3 m, and V_{pm} at intervals of 3 m s⁻¹ (b), at 00 UTC on*
473   *20 December, 2009. In (b), the "L" marks the satellite-derived surface cyclone center. From ERA-5 reanalysis.*

3.5 The subtropical cyclone of January, 2023

476   The term "subtropical cyclone" has been used to describe a variety of surface flux-assisted
477   cyclonic storms that do not strictly meet the definition of a tropical cyclone. The term has an
478   official definition in the North Atlantic[5] but is used occasionally elsewhere, especially in regions
479   where terms like medicane, polar low, and Kona storm do not apply, such as the South Atlantic
480   (Evans and Braun, 2012; Gozzo et al., 2014). Here we will use the term to designate CYCLOPs
481   in the sub-arctic North Atlantic; that is, surface flux-powered cyclones that develop in regions

---

[5] The National Hurricane Center defines a "subtropical cyclone" as "a non-frontal low-pressure system
that has characteristics of both tropical and extratropical cyclones", but in the past has also used the
terms "hybrid storm" and "neutercane".

482   and times whose climatological thermodynamic potential is small or zero, that would not be
483   called polar lows owing to their latitude. This usage may not be consistent with other definitions.
484   The point here is to show that CYCLOPs can occur in the North Atlantic and we can safely refer
485   to these as CYCLOPs whether or not they meet some definition of "subtropical cyclone".

486   Figure 17 displays a visible satellite image of a subtropical cyclone over the western North
487   Atlantic on 16 January, 2023. It resembles the medicanes and polar lows described previously,
488   and like them, formed under a cutoff cyclone aloft.

489
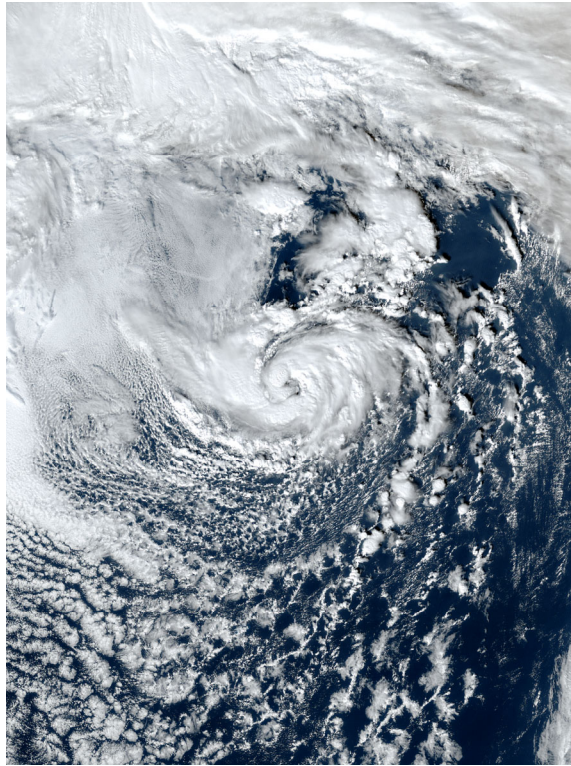
490   *Figure 17: Subtropical cyclone over the western North Atlantic, 18:20 UTC, 16 January 2023. NOAA geostationary*
491   *satellite image.*

492   The formation of the cutoff cyclone aloft is shown in Figure 18. A deep trough advances slowly
493   eastward over eastern North America and partially cuts off on the 14th. As the associated cold
494   pool and region of light shear migrate out over the warm waters south of the Gulf Stream, a
495   CYCLOP forms and intensifies with peak winds of around 60 kts at around 00 UTC on the 17th
496   (Cangliosi et al., 2023). Note also the anticyclonic wave breaking event to the east of the
497   surface cyclone development, in the eastern half of panels 18b-d.

498   The evolutions of the 950 hPa and associated V_{pm} fields are displayed in Figure 19. (Note the
499   smaller scale around the developing surface cyclone, compared to Figure 18.) On January 14th,
500   the only appreciably large values of V_{pm} are associated with the Gulf Stream and in the far
501   southwestern portion of the domain. The 950 hPa height field shows a broad trough associated

502 with the baroclinic wave moving slowly eastward off the U.S. east coast. But as the upper cold
503 cyclone moves out over warmer water on the 15th, large V_{pm} develops south of the Gulf Stream,
504 and a closed and more intense surface cyclone develops under the lowest 400 hPa heights and
505 over the region with higher V_{pm} values.

506

507
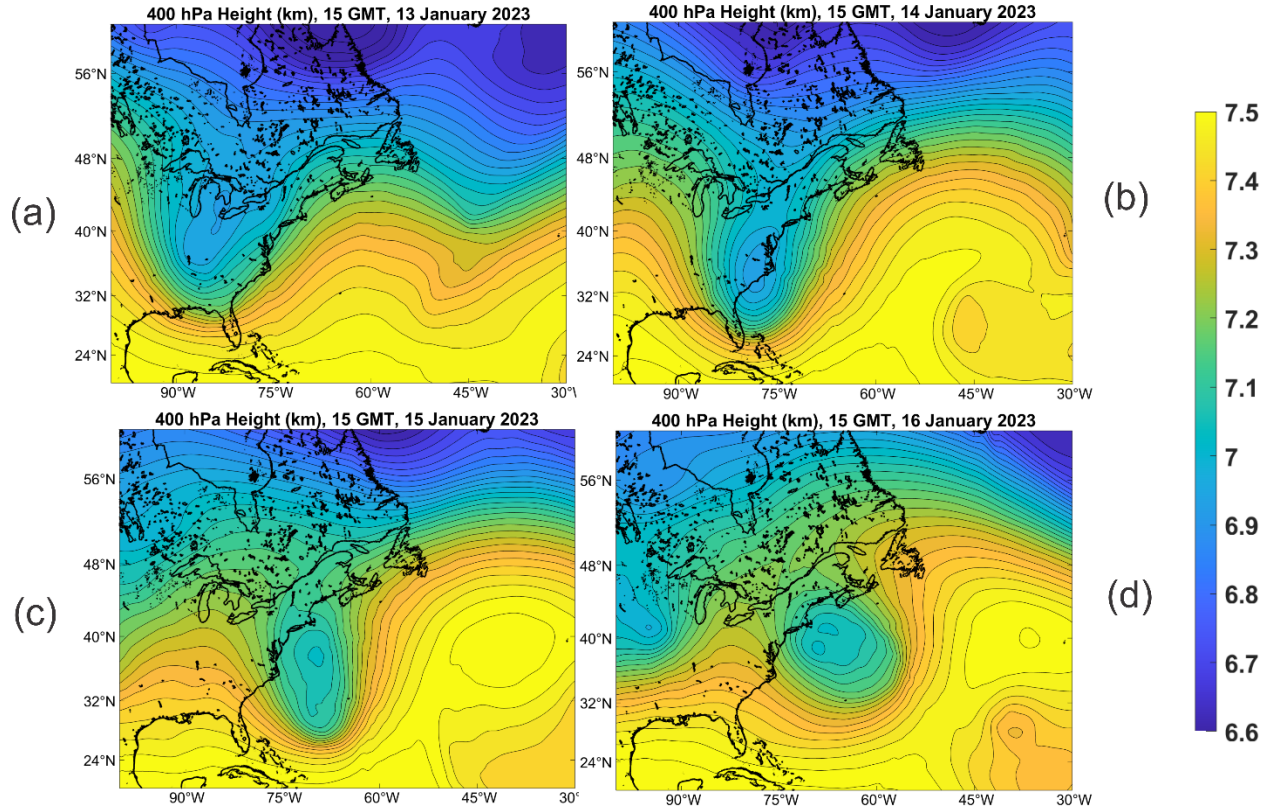
508 *Figure 18: 400 hPa geopotential height (km) at intervals of 30 m, at 15:00 UTC on January 13th (a), 14th (b), 15th (c),*
509 *and 16th (d), 2023. From ERA-5 reanalysis.*
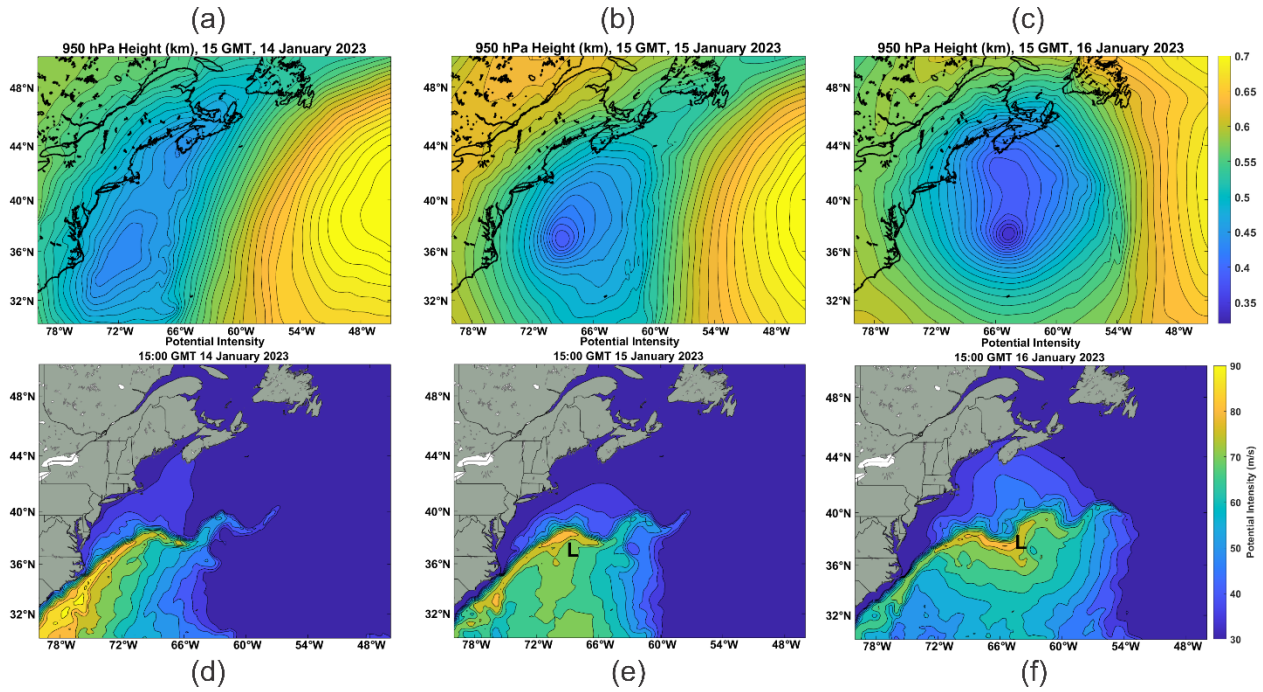
Figure 19: The 950 hPa geopotential height (km) at 15:00 UTC on January 14th (a), 15th (b), 16th (c); the V_{pm} field in increments of 5 ms^{-1}, on January 14th (d), 15th (e), and 16th(f). In (e) and (f) the "L" shows the position of the 950 hPa cyclone center at the time of the chart. From ERA-5 reanalysis.

As the upper tropospheric cyclone begins to pull out toward the northeast on the 16th, the surface cyclone intensifies in the region of large V_{pm} south of the Gulf Stream, while the more gradual warming of the surface air in the region of small V_{pm} north of the Stream yields surface pressure falls, but not as concentrated and intense as in the CYCLOP to the south.

Although the evolution of the upper tropospheric cyclone differs in detail from the previously examined cases, and the sharp gradient of sea surface temperature across the north wall of the Gulfstream clearly plays a role here, in other respects the development of this subtropical cyclone resembles that of other CYCLOPs, developing in regions of substantial thermodynamic potential that result, at least in part, from cooling aloft on synoptic time and space scales.

3.6 A Kona Storm

Hawaiians use the term "Kona Storm" to describe cold-season storms that typically form west of Hawaii and often bring damaging winds and heavy rain to the islands. The term "Kona" translates to "leeward", which in this region means the west side of the islands. They may have been first described in the scientific literature by Daingerfield (1921). Simpson (1952) states that Kona Storms possess "cold-core characteristics, with winds and rainfall amounts increasing with distance from the low-pressure center and reaching a maxima at a radius of 200 to 500 mi. However, with intensification, this cyclone may develop warm-core properties, with rainfall and

532   wind profiles bearing a marked resemblance to those of the tropical cyclone." In general,
533   Simpson's descriptions of the later stages of some Kona Storms are consistent with them being
534   CYCLOPs. But it should be noted that the term is routinely applied to cold-season storms that
535   bring hazardous conditions to Hawaii regardless of whether they have developed warm cores. A
536   good review of the climatology of Kona storms is provided by Otkin and Martin (2004), who state
537   that "development of the surface cyclone in all types results from the intrusion of an upper-level
538   disturbance of extratropical origin into the subtropics". Here we focus on Kona storms that do
539   develop warm cores, providing as a first example the Kona Storm of 19 December 2010. A
540   visible satellite image of this storm is shown in Figure 20.

541
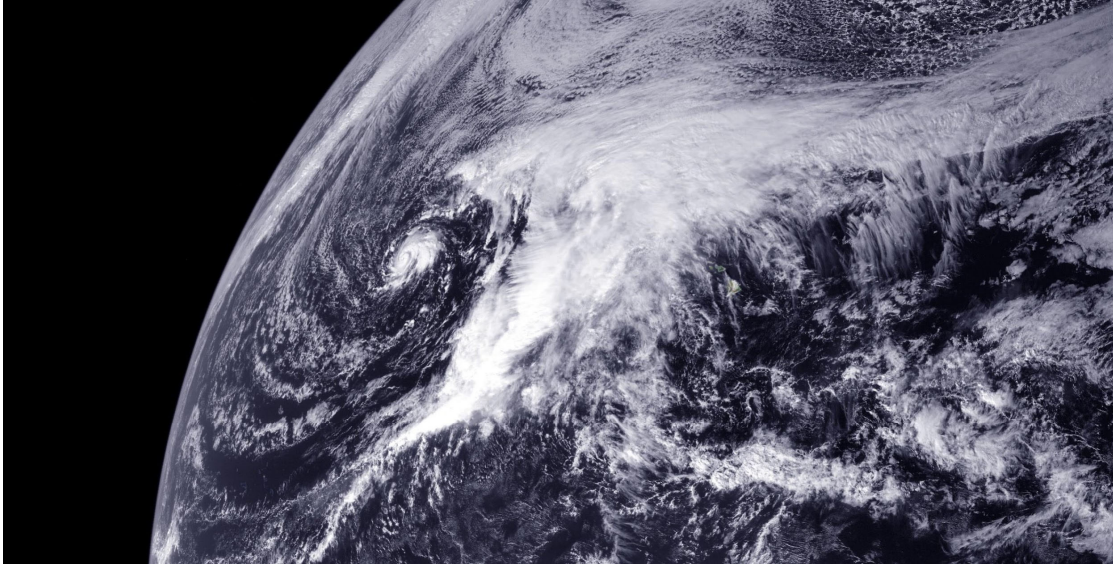
542   *Figure 20: Geostationary satellite visible image showing a Kona Storm at 00 UTC on 19 December 2010. The Kona*
543   *Storm is the small-scale cyclone left of the major cloud mass. (Image credit: NOAA-NASA GOES Project, 2010.)*

544
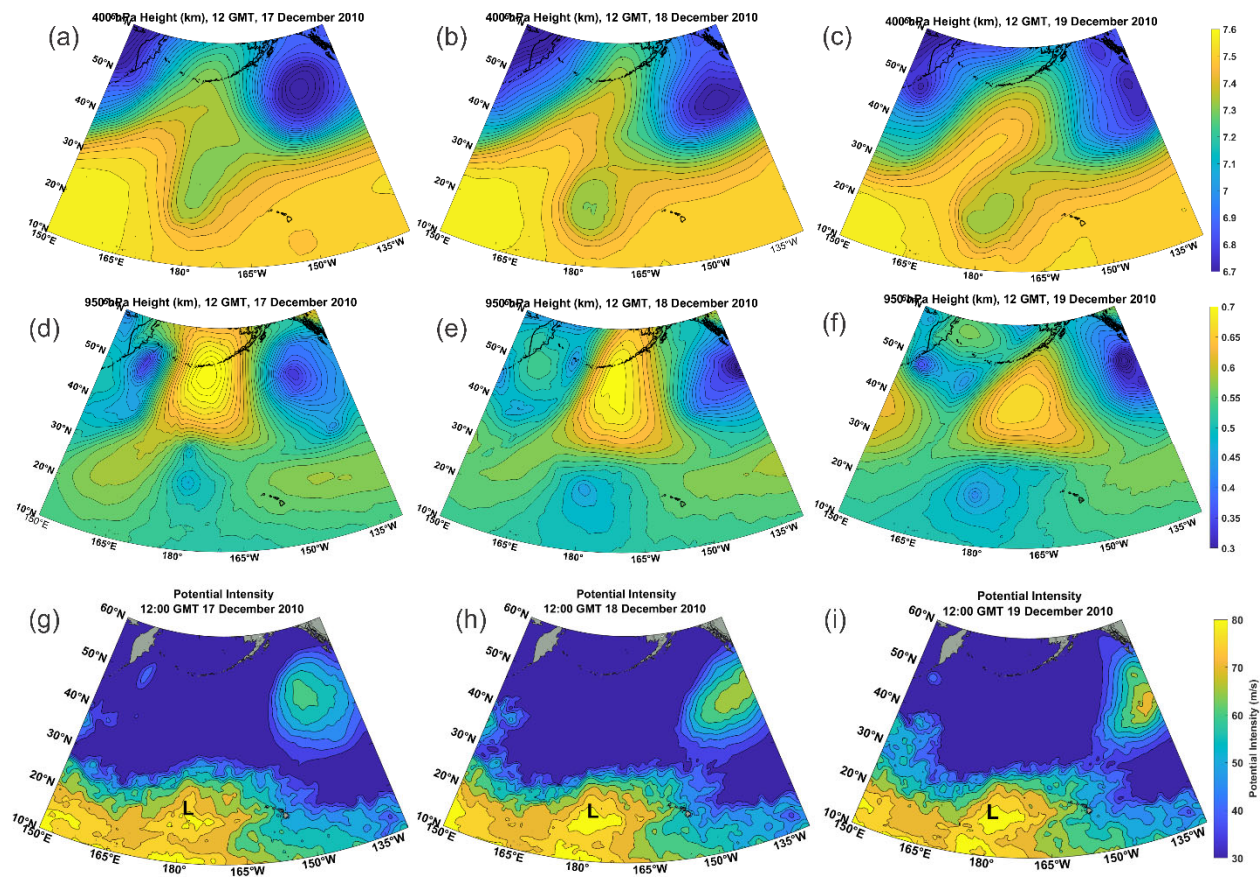
Figure 21: Sequence of 400 hPa geopotential height charts (km) at contour intervals of 30 m (a)-(c)), 950 hPa geopotential heights (km) with contour intervals of 13.34 m (d)-(f)), and V_{pm} with contour intervals of 5 ms^{-1} ((g)-(i)) at 12:00 UTC on December 17th ((a), (d), (g)), December 18th ((b), (e), (h)), and December 19th ((c), (f), (i)) 2010. The "L"s in ((g)-(i)) denote the positions of the 950 hPa cyclone center. From ERA-5 reanalysis.

As with all known CYCLOPs, the December 2010 Kona Storm developed under a cold-core cutoff cyclone aloft, as shown in Figure 21. The upper-level cyclone had a long and illustrious history before December 18th, having meandered over a large swath of the central North Pacific. But beginning on December 17th, the cutoff cyclone made a decisive swing southward over waters with higher values of V_{pm}. A broad surface cyclone was present underneath the cold pool aloft on all three days, but developed a tight inner core on the 19th as the cold pool slowly drifted over a region of higher potential intensity.

This Kona Storm developed in a region of modest climatological potential intensity that was, however, substantially enhanced by the cutoff cyclone aloft. For example, on December 17th, the conventional (unmodified) potential intensity at the position of the 950 hPa cyclone center was about 55 ms^{-1}, compared to the 75-80 ms^{-1} values of the modified potential intensity. One can only speculate whether a surface flux-driven cyclone would have developed without the enhanced cooling associated with the cutoff cyclone aloft.

562   This Kona storm was identified as a tropical storm by the Central Pacific Hurricane Center, as of
563   0900 UTC 20 December, and given the name Omeka.

564   The Kona Storm of March, 1951 is a more unambiguous case of a CYCLOP. Figure 22 shows
565   the 950 hPa geopotential height field on March 26, 1951. The storm, at that time, was classified
566   by the Joint Typhoon Warning Center as a tropical cyclone, but the climatological potential
567   intensity there at that time of year could not have supported any tropical cyclone. Figure 22c
568   shows that substantial V_{pm} was associated with a cutoff cyclone in the upper troposphere,
569   making possible the existence of this CYCLOP.
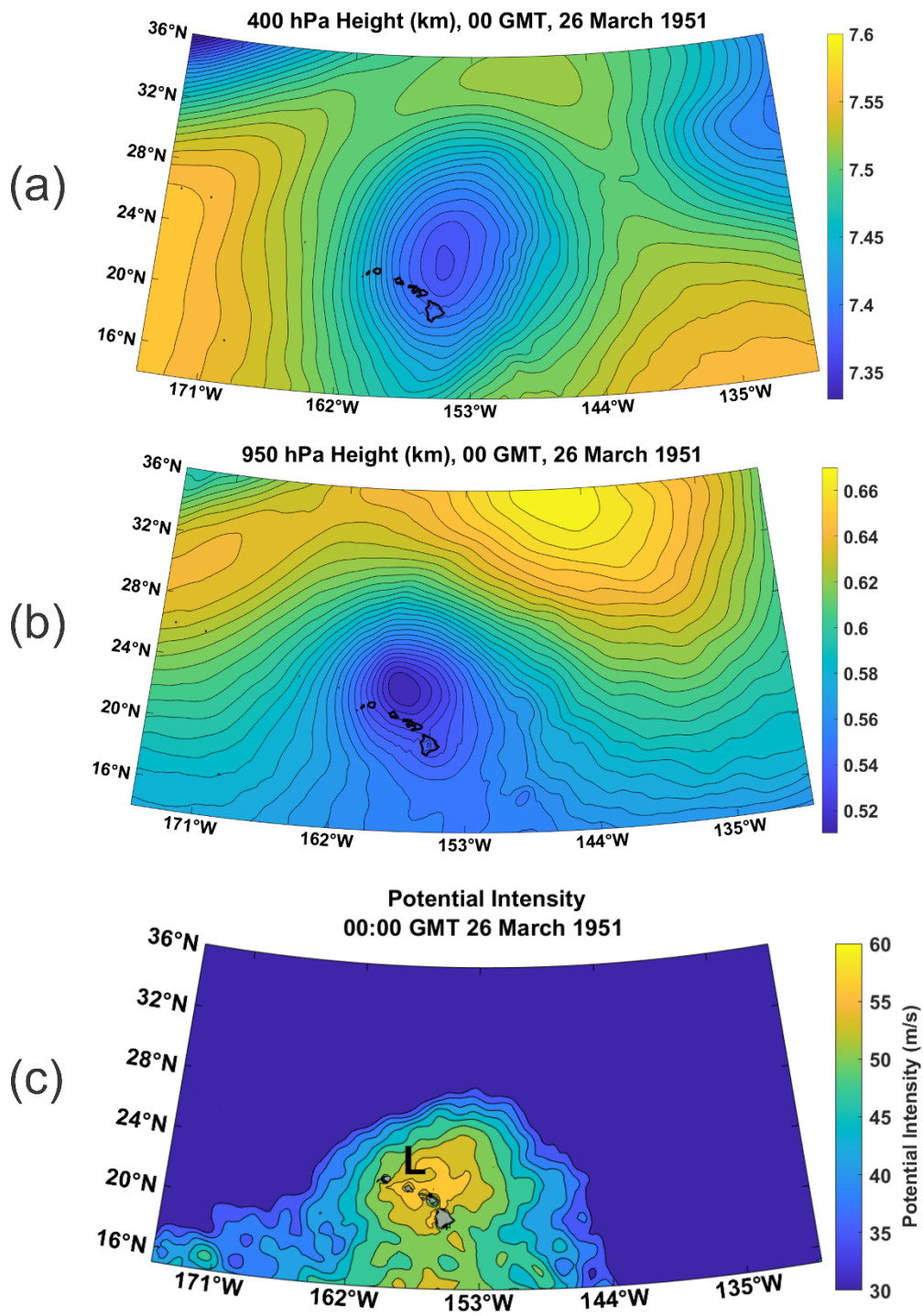
Figure 22: Kona Cyclone of March, 1951. Fields are shown at 00 UTC on 26 March: a): 400 hPa geopotential height (km)with a 10 m contour interval, b): 950 hPa geopotential height (km) with 5m contour interval, and c): V_{pm} with a contour interval of 3 ms^{-1}.

4. Variations on the Theme

We here are attempting to distinguish a class of cyclones, CYCLOPs, from other cyclonic storms by the physics of their development, not by the regions in which they develop. Here we present a case of an actual tropical cyclone in the Mediterranean that we do not identify as a CYCLOP.

4.1 Cyclone Zorbas

The cyclone known as Zorbas developed just north of Libya on 27 September 2018 and moved northward and then northeastward across the Peloponnese and the Aegean (Figure 23), dissipating in early October. The storm killed several people and did millions of dollars of damage.

Figure 23: Track of Cyclone Zorbas, from 27 September through 2 October, 2018. (Image credit: Wikipedia Commons; https://commons.wikimedia.org/wiki/File:Zorbas_2018_track.png)

The antecedent (actual, not modified) potential intensity distribution, on 26 September, is displayed in Figure 24. In much of the southern part of the central Mediterranean, the potential intensity was typical of tropical warm pools with values approaching 80 ms^{-1}. As with most medicanes, Zorbas was triggered by an upper tropospheric Rossby wave breaking event (Figure 25), but in this case the cold pool aloft only enhanced the existing potential intensity by about 7 ms^{-1} (on September 27th). In this case, the maximum 400 hPa geopotential perturbation was around 1500 m^{2}s^{-2}, compared to about 2500 m^{2}s^{-2} in the case of Medicane Zeo of 2005. Zorbas was therefore more like a classic case of a tropical cyclone resulting from tropical transition (Bosart and Bartlo, 1991; Davis and Bosart, 2003, 2004) and we might not describe it as a CYCLOP. Note that while the approach of the upper-level cyclone did not appreciably alter the potential intensity, it almost certainly humidified the middle troposphere, making genesis somewhat more likely, as may be true in most cases of tropical transition.
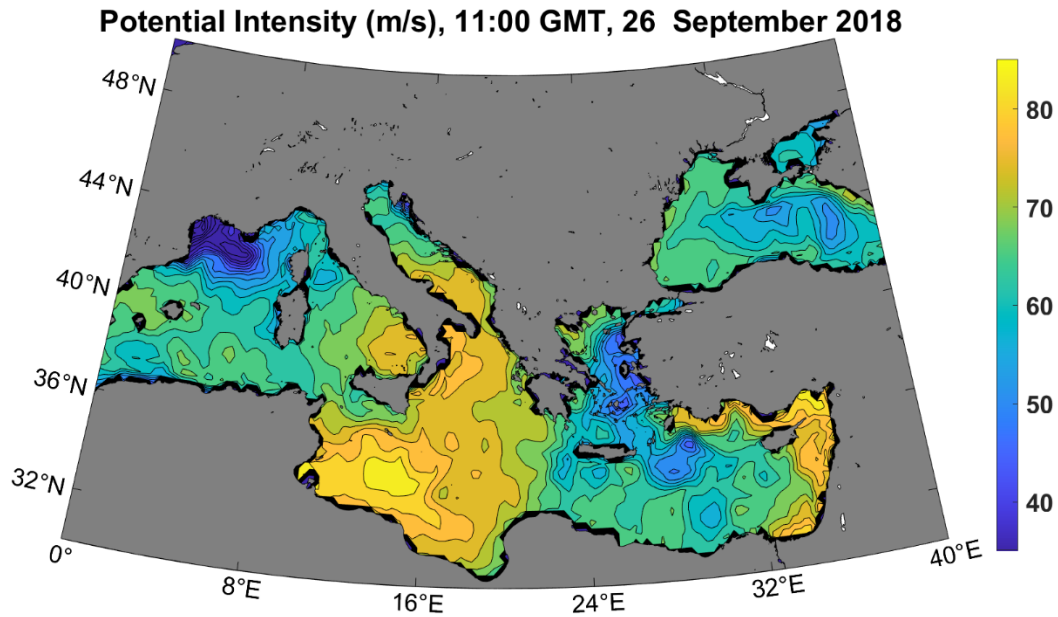
Figure 24: Actual potential intensity distribution in the Mediterranean and Black Seas, 11 UTC on 26 September 2018.
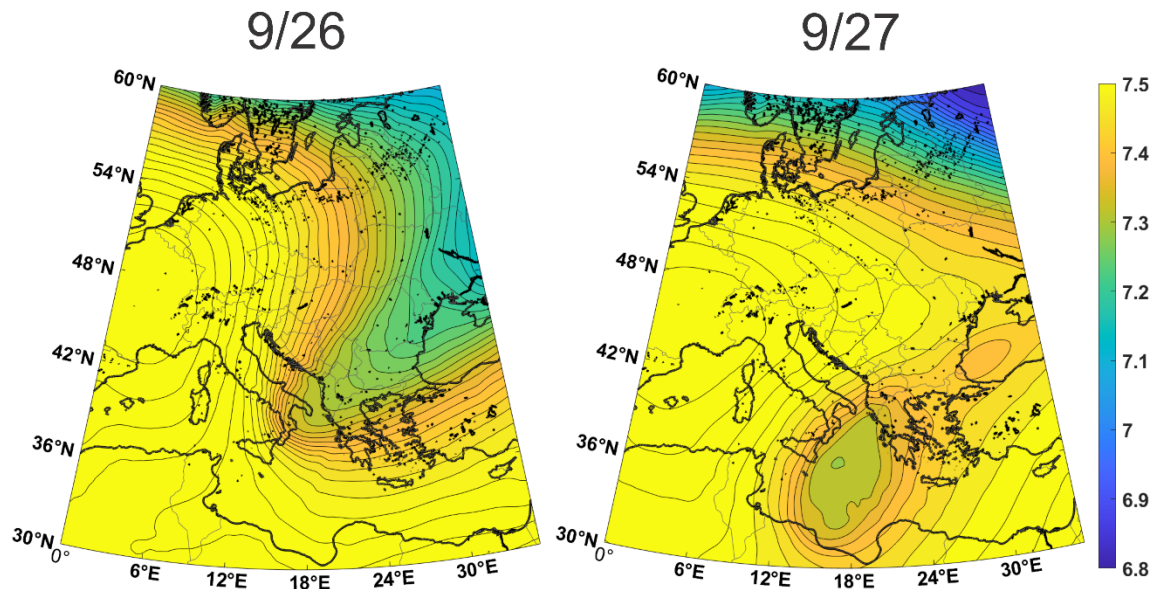
Figure 25: 400 hPa geopotential height (km) at 11 UTC on 26 September (left) and 27 September (right), 2018. Contour interval is 13.34 m. From ERA-5 reanalysis.

4.2 Cyclone Daniel

Cyclone Daniel of 2023 was the deadliest Mediterranean surface flux-driven cyclone in recorded history, with a death toll exceeding 4,000 and thousands of missing persons, mostly owing to floods caused by the catastrophic failure of two dams near Derna, Libya (Flaounas et al., 2024).

611   This flooding was the worst in the recorded history of the African continent. Figure 26 shows the
612   track of Daniel's center and a visible satellite image of the storm as it approached landfall in
613   Libya is shown in Figure 27. Daniel became a surface flux-driven cyclone off the west coast of
614   the Peloponnese on September 5th, made landfall near Benghazi, Libya, on September 10th and
615   dissipated over Egypt on the 12th.
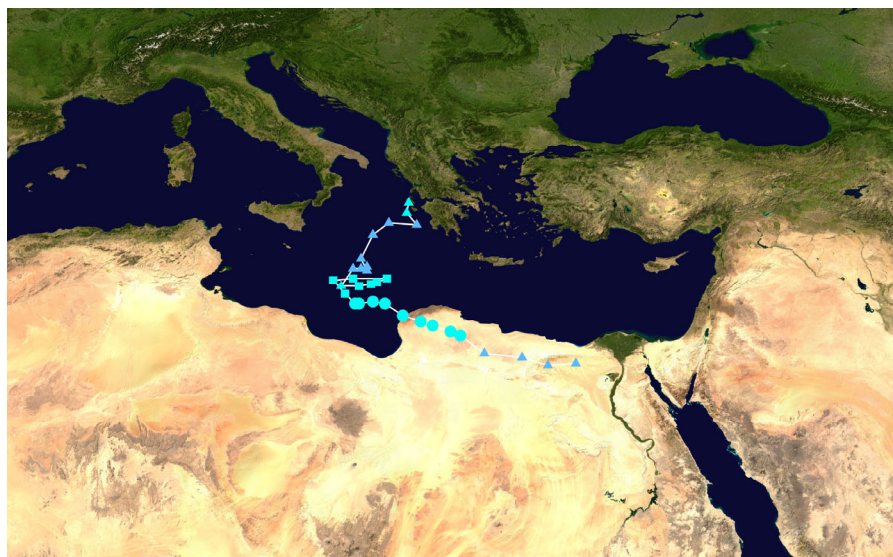
616

617   *Figure 26: Track of Storm Daniel at 6-hour intervals, beginning September 5th and ending September 12th, 2023. The*
618   *circles, squares and triangles along the track denote tropical cyclone, subtropical cyclone and extratropical cyclone*
619   *designations, respectively, while the deep blue and light blue colors denote tropical depression- and tropical storm-*
620   *force winds. (Image credit: Wikipedia commons; https://commons.wikimedia.org/wiki/File:Daniel_2023_track.png)*

621
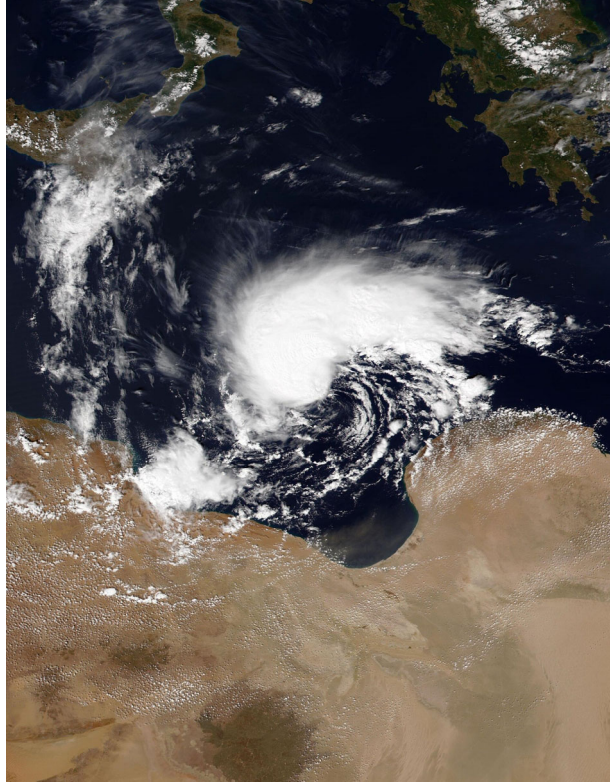
622   *Figure 27: NOAA-20 VIIRS image of Storm Daniel at 12 UTC 9 September 2023, as it approached the Libyan coast.*

623

624   As with Zorbas, the antecedent potential intensity was high throughout the Mediterranean south
625   and east of Italy and Sicily, and the event was triggered by a Rossby wave breaking event
626   (Figure 28). And as with Zorbas, the cutoff cyclone aloft was not strong enough to appreciably
627   alter the existing potential intensity but acted as a trigger for the tropical cyclone that Daniel
628   became. This was another classic case of tropical transition, and not a CYCLOP.

629
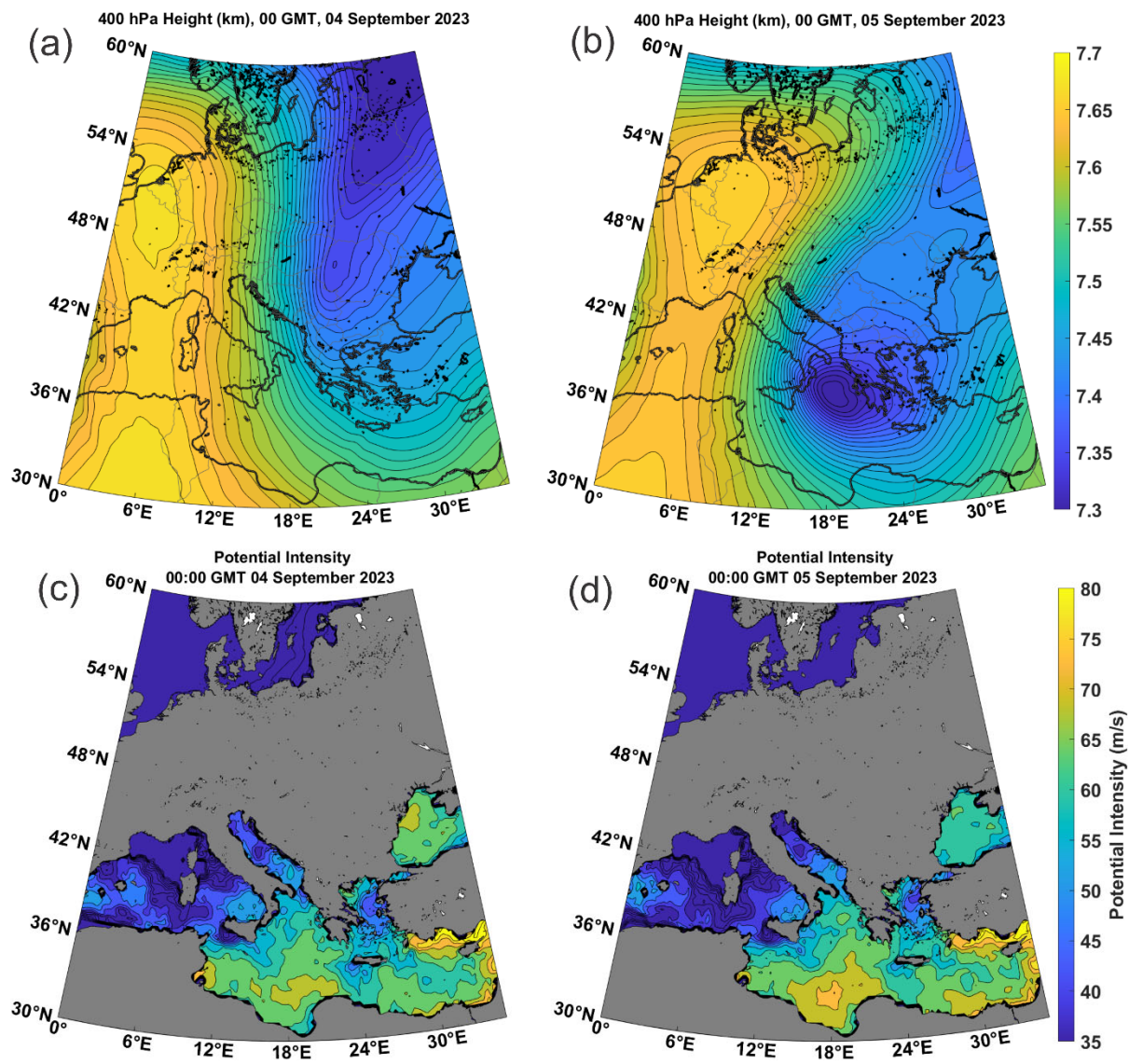
630   *Figure 28: 400 hPa geopotential height (km) with contour interval of 13.33 m (a)-(b); and actual potential intensity*
631   *(ms⁻¹) with contour interval of 4 ms⁻¹ (c)-(d) at 00 UTC September 4th ((a) and (c)) and 5th ((b) and (d)), from ERA-5*
632   *reanalyses.*

633   Yet Storm Daniel differed from Zorbas in one important respect: as it approached the Libyan
634   coast around September 10th, it came under the influence of strong high-level potential vorticity
635   (PV) advection owing to a mesoscale "satellite" PV mass rotating around the upper-level cutoff
636   cyclone (Figure 29). The quasi-balanced forcing associated with the superposition of the high-
637   level PV anomaly with the surface-based warm core probably contributed to Daniel's
638   intensification which, remarkably for a surface flux-driven cyclone, continued after landfall
639   (Hewson et al., 2024).

250 hPa Potential Vorticity (PV units), 12 GMT, 10 September 2023
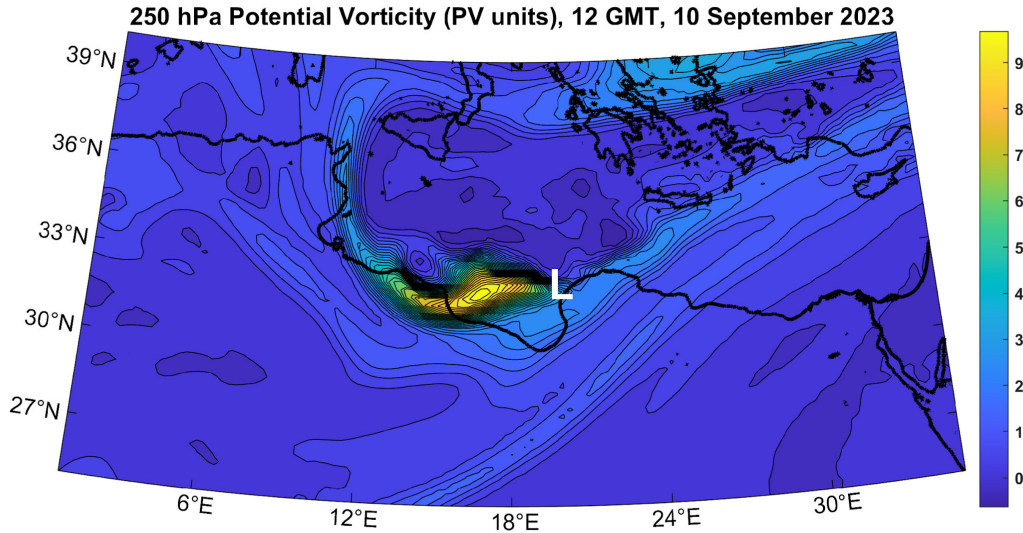
Figure 29: Potential vorticity (PV units, 10^{-6} K kg^{-1} m^2 s^{-1}) at 250 hPa at 12 UTC on 10 September, 2023. The white "L" marks the approximate surface center of Daniel at this time.

5. Summary and conclusions

We here argue that many of the cyclonic storms called medicanes, polar lows, subtropical cyclones, and Kona storms operate on the same physics and ought to be identified as a single class of storms that we propose to call CYCLOPs. In their developed structure and intensity they are essentially identical to tropical cyclones, and like TCs are driven primarily by wind-dependent surface enthalpy (latent and sensible heat) fluxes, but unlike classical TCs, there is little or no climatological potential intensity for the storms. Rather, the development and/or migration over relatively warm water of strong, cold-core cyclones in the upper troposphere cools and moistens the column through dynamical lifting, generating mesoscale to synoptic scale columns with elevated potential intensity and humidity, and reduced wind shear – ideal embryos for the development of surface flux-driven cyclones.

We do not expect CYCLOPs to last as long as classical TCs. In the first place, the conditions that enable such storms are confined in space and transient in time. For example, the cutoff cyclone aloft is often re-absorbed into the main baroclinic flow. In addition, the strong surface enthalpy fluxes that power CYCLOPs also increase, through the action of deep convection, the enthalpy of the otherwise spatially limited cold columns in which they form, reducing over time the thermodynamic disequilibrium between the air column and the sea surface. A back-of-the-envelope estimate for the time to destroy the initial thermodynamic disequilibrium is on the order of days. By contrast, even the strongest classical TCs do not sufficiently warm the large expanses of the tropical troposphere they influence to appreciably diminish the large-scale potential intensity of tropical warm pools.

665 Not all cyclonic storms that have been called polar lows, medicanes, subtropical cyclones, or
666 Kona storms meet our definition of CYCLOP. The literature describes many polar lows that have
667 been traced to something more nearly like classical baroclinic instability acting in an air mass of
668 anomalously low static stability (e.g. Sardie and Warner, 1985). Many storms identified as Kona
669 storms because of their location and season, and which developed under cold cyclones aloft,
670 never received much of a boost from surface fluxes and therefore would not be classified as
671 CYCLOPs. And, as we described in the last section, two strong Mediterranean cyclones, Zorbas
672 of 2018 and Daniel of 2023, developed in environments of high climatological potential intensity
673 and formed via the tropical transition process.

674 Beyond these caveats, not all cold-core, closed cyclones in the upper troposphere that develop
675 or move over relatively warm ocean waters develop CYCLOPs. Without doing a comprehensive
676 survey, we have found several cases of greatly enhanced potential intensity under cold lows
677 aloft that did not develop strong, concentrated surface cyclones. We suspect that, as with
678 classical tropical cyclones, dry air incursions above the boundary layer may have prevented
679 genesis in these cases, but as these events generally occur in regions devoid of in-situ
680 observations, it is not clear how well reanalyses capture variations of moisture on the scale of
681 CYCLOPs. In any event, the efficiency with which upper-level cut-off cyclones produce
682 CYCLOPs, given a substantial perturbation in potential intensity, should be a subject of future
683 research.

684 Clearly, there exists a continuum between pure tropical transition, in which synoptic-scale
685 dynamics play no role in setting up the potential intensity, and pure CYCLOPs in which
686 synoptic-scale processes create all the potential intensity that drives the storm. The distinction
687 we are making here does not pertain to the final result – a tropical cyclone[6] – but to the route to
688 creating it. As a practical matter, forecasters should consider both the triggering potential and
689 mesoscale to synoptic scale environmental development in predicting the formation and
690 evolution of CYCLOPs. The modified potential intensity (V_{pm}) introduced here may prove to be
691 a valuable diagnostic that can easily be calculated from NWP model output. To simulate
692 CYCLOPs, NWP models need to make accurate forecasts of dynamic processes that lead to
693 the formation and humidification of deep cold pools aloft, and be able to handle surface fluxes
694 and other boundary layer processes essential to the formation of surface flux-driven cyclones.
695 And, as with tropical cyclones, coupling to the ocean is essential for accurate intensity
696 prediction.

697 Finally, we encourage researchers to focus on the essential physics of CYCLOP development
698 regardless of where in the world they occur. Casting a broader geographical net will harvest a
699 greater sample of such storms and should lead to more rapid progress in understanding and
700 forecasting them.

---

[6] It might be beneficial to develop a term that generically denotes a cyclone driven primarily by surface enthalpy fluxes. "Tropical cyclone" seems unsuited to the task, since "tropical" hardly describes, e.g., a polar low. Such a generic term would encompass both conventional tropical cyclones, which occur in regions of climatologically large potential intensity, and CYCLOPs, for which potential intensity is generated locally in space and time.

701

Appendix

703 CYCLOPs form when dynamical processes create synoptic-scale cold columns marked by
704 cutoff cyclones in the upper troposphere. The objective here is to calculate tropical cyclone
705 potential intensity in these cold columns. The problem is that the CYCLOPs themselves, and
706 surface heat fluxes in general, warm the columns, sometimes rapidly, diminishing the potential
707 intensity. We want to know what the potential intensity was before this warming occurs. Here we
708 develop a modified potential intensity using the surface pressure depression as proxy for the
709 column heating.

710 Potential intensity is a measure of the maximum surface wind speed that can be achieved by a
711 cyclone fueled entirely by surface enthalpy fluxes. It is defined (see Rousseau-Rizzi and
712 Emanuel (2019) for an up-to-date definition):

713
$$V_p^2 = \frac{C_k}{C_D} \frac{T_s - T_o}{T_o} \left(h_0^* - h_b \right),$$
(A1)

714 Where C_k and C_D are the surface exchange coefficients for enthalpy and momentum, T_s and

715 T_o are the absolute temperatures of the surface and outflow layer, h_0^* is the saturation moist

716 static energy of the sea surface, and h_b is the moist static energy of the boundary layer.

717 Using the relation $T\delta s \simeq \delta h$, where s is moist entropy, we can re-write (A1) slightly as

718
$$V_p^2 = \frac{C_k}{C_D} \frac{T_s - T_o}{T_o} T_s \left(s_0^* - s_b \right).$$
(A2)

719 Next, we assume that the troposphere near CYCLOPs has a nearly moist adiabatic lapse rate[7],
720 and the moist entropy of the boundary layer is equal to the saturation moist entropy, s^*, of the
721 troposphere; i.e., that the troposphere is neutrally stable to moist adiabatic ascent from the
722 boundary layer. Under these conditions, (A2) may be re-written

723
$$V_p^2 = \frac{C_k}{C_D} \frac{T_s - T_o}{T_o} T_s \left(s_0^* - s^* \right).$$
(A3)

---

[7] If the lapse rate is appreciably sub-adiabatic, then convection cannot occur and no flux-driven cyclone could develop. This condition would be associated with a larger value of s* in (A3), which would at least reduce the calculated value of V_p. Super-adiabatic lapse rates are not generally observed over the ocean within deep humid layers.

724 Here s^* is constant with altitude, since the troposphere is assumed to have a moist adiabatic
725 lapse rate.

726 Referring to Figure 1a in the main text, we want to know what the potential intensity is in the
727 vicinity of the cutoff cyclone aloft *before* the atmosphere underneath it has started to warm up
728 under the influence of surface enthalpy fluxes. But in reality, this warming commences as soon
729 as the system moves over relatively warm water and deep convection begins. We can estimate
730 what the temperature, or s^*, was before the warming began by using the surface pressure drop
731 as a proxy for the column warming.

732 We begin with the perturbation hydrostatic equation in pressure coordinates:

$$\frac{\partial \phi'}{\partial p} = -\alpha', \tag{A4}$$

734 where ϕ' is the perturbation geopotential and α' is the perturbation specific volume. Since the
735 latter is a function of pressure and s^* only, we can use the chain rule and one of the Maxwell
736 relations from thermodynamics (Emanuel, 1994) to write (A4) as

$$\frac{\partial \phi'}{\partial p} = -\left(\frac{\partial T}{\partial p}\right)_{s^*} s^{*'}. \tag{A5}$$

738 Now, since $s^{*'}$ does not vary with altitude, we can integrate (A5) from the surface to the local
739 tropopause to yield

$$-\phi_s' = \left(T_s - T_{\phi'=0}\right) s^{*'}. \tag{A6}$$

741 where ϕ_s' is the near-surface geopotential perturbation and $T_{\phi'=0}$ is the absolute temperature at
742 the level where the CYCLOP-induced geopotential perturbation vanishes.

743 Therefore the CYCLOP-induced warming of the troposphere is estimated as

$$s^{*'} = \frac{-\phi_s'}{T_s - T_{\phi'=0}}. \tag{A7}$$

745 We subtract this warming from the reanalysis environmental saturation entropy in (A3), yielding

$$V_{pm}^2 = \frac{C_k}{C_D} \frac{T_s - T_o}{T_o} T_s \left(s_0^* - s_e^* - \frac{\phi_s'}{T_s - T_{\phi'=0}}\right), \tag{A8}$$

747 where s_e^* is the analyzed saturation entropy of the column. This can be written alternatively as

748
$$V_{pm}^2 = V_p^2 - \frac{C_k}{C_D} \frac{T_s}{T_o} \frac{T_s - T_o}{T_s - T_{\phi'=0}} \phi_s',$$ (A9)

749 where V_p is the ~~unperturbed~~ potential intensity calculated from the reanalysis. We use (A9) in

750 the calculations reported in this paper, with V_p calculated using the algorithm of Bister and

751 Emanuel (2002).

752 For the purposes of the present work, we defined the perturbation as the difference between the
753 actual geopotential and its climatological value determined from monthly mean values over the
754 period 1979-2023, and we estimate the near-surface cyclone geopotential perturbation as that
755 at 950 hPa. In (A9), we do not know the precise value of C_k / C_D, but it should be of order unity
756 and is generally assumed as such when potential intensity is calculated in practice (e.g.
757 Emanuel, 2000). The surface temperature, T_s, should be captured well in reanalyses, while the
758 outflow temperature is often taken as the local unperturbed tropopause temperature (Emanuel,
759 2000). In general, the pressure perturbation associated with tropical cyclones changes sign
760 somewhere in the upper troposphere, and for simplicity we take $T_{\phi'=0} = T_o$ here.   In the tropics,
761 the surface temperature can be around 300 K while the tropopause is often as cold as 200K,
762 yielding $T_s / T_o = 1.5$, while in polar latitudes, the surface temperature can be just above
763 freezing (273 K) while the tropopause is warmer, around 220 K, giving $T_s / T_o = 1.25$. As in any
764 case C_k / C_D is uncertain, we take $T_s / T_o = 1.3$ here for simplicity, and approximate (A9) as

765
$$V_{pm}^2 = V_p^2 - 1.3 \phi_s'.$$ (A10)

766 The contribution of the last term in (A10) is usually small except in the immediate vicinity of a
767 CYCLOP.

768 The individual contributions of the two terms on the right side of (A10) are displayed in Figure
769 A1, which pertains to the case of Medicane Celeno on the 14th and 15th of January, 1995. The
770 total (modified) potential intensity for these two dates and times is shown in Figure 5 *g* and *h*. In
771 general, the contribution of the correction (last term in (A10)) is modest.

772 Code and data availability

773 No modeling was performed in the course of this work, and no code developed except to plot
774 reanalysis data. Routines for calculating potential intensity are available at
775 https://github.com/dgilford/tcpyPI . All of the meteorological analyses presented herein are
776 based in ERA5 downloaded from the Copernicus Climate Change Service
777 (https://doi.org/10.24381/cds.143582cf, Hersbach et al., 2020).

778 Author contributions

779 KE carried out the analyses and prepared the manuscript with contributions from all the co-
780 authors.

781
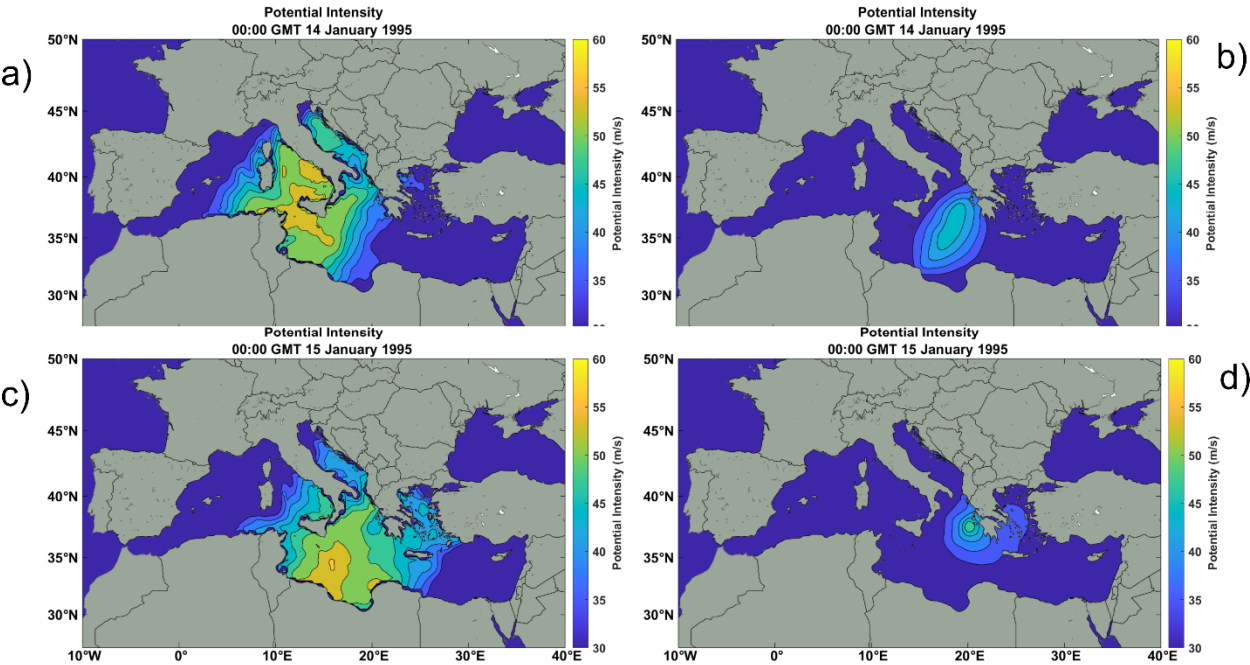
782 *Figure A1: Unmodified potential intensity (a and c) and modification of the potential intensity (b and d) at 00 UTC on*
783 *January 14th (a and b) and 15th (c and d). Note that the full modified potential intensity is not the arithmetic sum of*
784 *these two contributions but rather their Euclidean norm.*

785 Competing interests

786 The authors declare that they have no conflict of interest.

Acknowledgements

788 We thank two anonymous reviewers for most helpful and conscientious reviews, and Lance
789 Bosart for his detailed and highly constructive comments.

790 This paper was motivated by discussions at the TROPICANA (TROPIcal Cyclones in
791 ANthropocene: physics, simulations & Attribution) program, which took place in June 2024 at
792 the Institute Pascal, University of Paris-Saclay, and aimed to address complex issues related to
793 tropical cyclones, medicanes, and their connection with climate change.

794 This work was made possible by Institut Pascal at Université Paris-Saclay with the support of
795 the program TROPICANA, "Investissements d'avenir" ANR-11-IDEX-0003-01.

796 T. Alberti and D. Faranda acknowledge useful discussions within the MedCyclones COST
797 Action (CA19109) and the FutureMed COST Action (CA22162) communities.

798 S. Bourdin received financial support from the NERC-NSF research grant n° NE/W009587/1
799 (NERC) & AGS-2244917 (NSF) HUrricane Risk Amplification and Changing North Atlantic
800 Natural disasters (Huracan), and from the EUR IPSL-Climate Graduate School through the
801 ICOCYCLONES2 project, managed by the ANR under the "Investissements d'avenir"
802 programme with the reference 37 ANR-11-IDEX-0004 - 17-EURE-0006.

803 S.J. Camargo and C.-Y. Lee acknowledge the support of the U.S. National Science Foundation
804 (AGS 20-43142, 22-17618, 22-44918) and U.S. Department of Energy (DOE) (DE-
805 SC0023333).

806 D. Faranda, E. Flaounas were supported by the COST Action CA22162 - FutureMed: A
807 TRANSDISCIPLINARY NETWORK TO BRIDGE CLIMATE SCIENCE AND IMPACTS ON
808 SOCIETY (FutureMed).

809 K. Emanuel was supported by the U.S. National Science Foundation under grant AGS-2202785.

810 J.J. González-Alemán thanks support from AEMET and from the Spanish PID2023-146344OB-
811 I00 project, funded by MICIU/AEI/10.13039/501100011033 y by FEDER, EU

812 M. M. Miglietta was partly supported by "Earth Observations as a cornerstone to the
813 understanding and prediction of tropical like cyclone risk in the Mediterranean (MEDICANES)",
814 ESA Contract No. 4000144111/23/I-KE.

815 H. Ramsay acknowledges funding support from the Australian Climate Service and the Climate
816 Systems Hub of the Australian Government's National Environmental Science Program (NESP).

817 M. Reale was supported by the National Recovery and Resilience Plan project TeRABIT
818 (Terabit network for Research and Academic Big data in Italy - IR0000022 - PNRR Missione 4,
819 Componente 2, Investimento 3.1 CUP I53C21000370006) in the frame of the European Union -
820 NextGenerationEU funding.

821 R. Romero acknowledges financial support by the "Ministerio de Ciencia e Innovación" of Spain
822 through the grant TRAMPAS (PID2020-113036RB-I00/AEI/10.13039/501100011033).

823

References

825 Betts, A. K.: A new convective adjustment scheme. Part I: Observational and theoretical basis.,
826 Quart J Roy Meteor Soc, 112, 677-691., 1986.

827 Bister, M. and Emanuel, K. A.: Low frequency variability of tropical cyclone potential intensity, 1:
828 Interannual to interdecadel variability, J Geophys Res, 107, doi:10.1029/2001JD000776, 2002.

829 Bosart, L. F. and Bartlo, J. A.: Tropical storm formation in a baroclinic environment, Mon Wea
830 Rev, 119, 1979–2013, 1991.

831   Cangliosi, J. P., Papin, P., and Beven, J. L.: Unnamed tropical storm (AL012023)., 2023.

832   Cavicchia, L., von Storch, H., and Gualdi, S.: A long-term climatology of medicanes, Clim. Dyn.,
833   43, 1183–1195, https://doi.org/10.1007/s00382-013-1893-7, 2014.

834   Cavicchia, L., Pepler, A., Dowdy, A., and Walsh, K.: A physically based climatology of the
835   occurrence and intensification of Australian East Coast Lows, J. Clim., 32, 2823–2841,
836   https://doi.org/10.1175/JCLI-D-18-0549.1, 2019.

837   Chavas, D. R. and Emanuel, K. A.: Equilibrium tropical cyclone size in an idealized state of
838   axisymmetric radiative–convective equilibrium, J Atmos Sci, 71, 1663–1680, 2014.

839   Cronin, T. W. and Chavas, D. R.: Dry and semidry tropical cyclones, J. Atmospheric Sci., 76,
840   2193–2212, https://doi.org/10.1175/jas-d-18-0357.1, 2019.

841   Daingerfield, L. H.: Kona storms, Mon. Weather Rev., 49, 327–329,
842   https://doi.org/10.1175/1520-0493(1921)49<327:ks>2.0.co;2, 1921.

843   Davis, C. A. and Bosart, L. F.: Baroclinically induced tropical cyclogenesis, Mon. Weather Rev.,
844   131, 2730–2747, https://doi.org/10.1175/1520-0493(2003)131<2730:BITC>2.0.CO;2, 2003.

845   Davis, C. A. and Bosart, L. F.: The TT problem: Forecasting the tropical transition of cyclones,
846   Bull. Am. Meteorol. Soc., 85, 1657–1662, https://doi.org/10.1175/BAMS-85-11-1657, 2004.

847   Emanuel, K.: Genesis and maintenance of "Mediterranean hurricanes," Adv Geosci, 2, 217–
848   220, 2005.

849   Emanuel, K.: Tropical cyclone activity downscaled from NOAA-CIRES reanalysis, 1908-1958, J
850   Adv Model Earth Sys, 2, 1–12, 2010.

851   Emanuel, K. A.: Atmospheric Convection, Oxford Univ. Press, New York, 580 pp., 1994.

852   Emanuel, K. A.: Some aspects of hurricane inner-core dynamics and energetics., J Atmos Sci,
853   54, 1014–1026, 1997.

854   Emanuel, K. A.: A statistical analysis of tropical cyclone intensity, Mon Wea Rev, 128, 1139–
855   1152, 2000.

856   Emanuel, K. A., Neelin, J. D., and Bretherton, C. S.: On large-scale circulations in convecting
857   atmospheres, Quart J Roy Meteor Soc, 120, 1111–1143, 1994.

858   Evans, J. L. and Braun, A.: A climatology of subtropical cyclones in the South Atlantic, J. Clim.,
859   25, 7328–7340, https://doi.org/10.1175/JCLI-D-11-00212.1, 2012.

860   Fantini, M.: The influence of heat and moisture fluxes from the ocean on the development of
861   baroclinic waves, J. Atmospheric Sci., 47, 840–855, https://doi.org/10.1175/1520-
862   0469(1990)047<0840:TIOHAM>2.0.CO;2, 1990.

863 Fita, L. and Flaounas, E.: Medicanes as subtropical cyclones: the December 2005 case from
864 the perspective of surface pressure tendency diagnostics and atmospheric water budget, Q. J.
865 R. Meteorol. Soc., 144, 1028–1044, https://doi.org/10.1002/qj.3273, 2018.

866 Flaounas, E., Dafis, S., Davolio, S., Faranda, D., Ferrarin, C., Hartmuth, K., Hochman, A.,
867 Koutroulis, A., Khodayar, S., Miglietta, M. M., Pantillon, F., Patlakas, P., Sprenger, M., and
868 Thurnherr, I.: Dynamics, predictability, impacts, and climate change considerations of the
869 catastrophic Mediterranean Storm Daniel (2023), EGUsphere, 2024, 1–29,
870 https://doi.org/10.5194/egusphere-2024-2809, 2024.

871 Gan, M. A. and Piva, E. D.: Energetics of southeastern Pacific cut-off lows, Clim. Dyn., 46,
872 3453–3462, https://doi.org/10.1007/s00382-015-2779-7, 2016.

873 Gozzo, L. F., Rocha, R. P. da, Reboita, M. S., and Sugahara, S.: Subtropical cyclones over the
874 southwestern South Atlantic: Climatological aspects and case study, J. Clim., 27, 8543–8562,
875 https://doi.org/10.1175/JCLI-D-14-00149.1, 2014.

876 Hersbach, H., Bell, B., Berrisford, P., Hirahara, S., Horányi, A., Muñoz-Sabater, J., Nicolas, J.,
877 Peubey, C., Radu, R., Schepers, D., Simmons, A., Soci, C., Abdalla, S., Abellan, X., Balsamo,
878 G., Bechtold, P., Biavati, G., Bidlot, J., Bonavita, M., De Chiara, G., Dahlgren, P., Dee, D.,
879 Diamantakis, M., Dragani, R., Flemming, J., Forbes, R., Fuentes, M., Geer, A., Haimberger, L.,
880 Healy, S., Hogan, R. J., Hólm, E., Janisková, M., Keeley, S., Laloyaux, P., Lopez, P., Lupu, C.,
881 Radnoti, G., de Rosnay, P., Rozum, I., Vamborg, F., Villaume, S., and Thépaut, J.-N.: The
882 ERA5 global reanalysis, Q. J. R. Meteorol. Soc., 146, 1999–2049,
883 https://doi.org/10.1002/qj.3803, 2020.

884 Hewson, T., Ashoor, A., Bousetta, S., Emanuel, K., Lagouvardos, K., Lavers, D., Magnusson,
885 L., Pillosu, F., and Zoster, E.: Medicane Daniel: an extraordinary cyclone with devastating
886 impacts, ECMWF Newsl., 179, 33–47, 2024.

887 Holland, G. J., Lynch, A. H., and Leslie, L. M.: Australian east-coast cyclones. Part I: Synoptic
888 overview and case study, Mon. Weather Rev., 115, 3024–3036, https://doi.org/10.1175/1520-
889 0493(1987)115<3024:AECCPI>2.0.CO;2, 1987.

890 Leutbecher, M. and Palmer, T. N.: Ensemble forecasting, Predict. Weather Clim. Extreme
891 Events, 227, 3515–3539, https://doi.org/10.1016/j.jcp.2007.02.014, 2008.

892 McIntyre, M. E. and Palmer, T. N.: Breaking planetary waves in the stratosphere, Nature, 305,
893 593–600, https://doi.org/10.1038/305593a0, 1983.

894 McTaggart-Cowan, R., Deane, G. D., Bosart, L. F., Davis, C. A., and Galarneau, T. J.:
895 Climatology of tropical cyclogenesis in the North Atlantic (1948–2004), Mon. Weather Rev., 136,
896 1284–1304, https://doi.org/10.1175/2007MWR2245.1, 2008.

897 McTaggart-Cowan, R., Galarneau, T. J., Bosart, L. F., Moore, R. W., and Martius, O.: A global
898 climatology of baroclinically influenced tropical cyclogenesis, Mon. Weather Rev., 141, 1963–
899 1989, https://doi.org/10.1175/MWR-D-12-00186.1, 2013.

900 McTaggart-Cowan, R., Davies, E. L., Fairman, J. G., Galarneau, T. J., and Schultz, D. M.:
901 Revisiting the 26.5°c sea surface temperature threshold for tropical cyclone development, Bull.
902 Am. Meteorol. Soc., 96, 1929–1943, https://doi.org/10.1175/BAMS-D-13-00254.1, 2015.

903 Miglietta, M. M. and Rotunno, R.: Development mechanisms for Mediterranean tropical-like
904 cyclones (medicanes), Q. J. R. Meteorol. Soc., 145, 1444–1460, https://doi.org/10.1002/qj.3503,
905 2019.

906 Nastos, P. T., Karavana Papadimou, K., and Matsangouras, I. T.: Mediterranean tropical-like
907 cyclones: Impacts and composite daily means and anomalies of synoptic patterns, High Impact
908 Atmospheric Process. Mediterr., 208, 156–166, https://doi.org/10.1016/j.atmosres.2017.10.023,
909 2018.

910 Nordeng, T. E. and Rasmussen, E. A. D.-:10. 1034/j. 1600-0870. 1992. 00001. x: A most
911 beautiful polar low. A case study of a polar low development in the Bear Island region, Tellus A,
912 44, 81–99, 1992.

913 Otkin, J. A. and Martin, J. E.: A synoptic climatology of the subtropical Kona storm, Mon.
914 Weather Rev., 132, 1502–1517, https://doi.org/10.1175/1520-
915 0493(2004)132<1502:ASCOTS>2.0.CO;2, 2004.

916 Pytharoulis, I., Craig, G. C., and Ballard, S. P.: Study of the Hurricane-like Mediterranean
917 cyclone of January 1995, Phys. Chem. Earth Part B Hydrol. Oceans Atmosphere, 24, 627–632,
918 https://doi.org/10.1016/S1464-1909(99)00056-8, 1999.

919 Romero, R. and Emanuel, K. D.-:10. 1002/jgrd. 50475: Medicane risk in a changing climate, J
920 Geophys Res, 118, 2013.

921 Rotunno, R. and Emanuel, K. A.: An air-sea interaction theory for tropical cyclones. Part II., J
922 Atmos Sci, 44, 542–561, 1987.

923 Rousseau-Rizzi, R. and Emanuel, K.: An evaluation of hurricane superintensity in axisymmetric
924 numerical models, J. Atmospheric Sci., 76, 1697–1708, https://doi.org/10.1175/jas-d-18-0238.1,
925 2019.

926 Sardie, J. M. and Warner, T. T. D.-:10. 1111/j. 1600-0870. 1985. tb00444. x: A numerical study
927 of the development mechanisms of polar lows, Tellus A, 37A, 460–477, 1985.

928 Simpson, R. H.: Evolution of the Kona storm: A subtropical cyclone, J. Atmospheric Sci., 9, 24–
929 35, https://doi.org/10.1175/1520-0469(1952)009<0024:EOTKSA>2.0.CO;2, 1952.

930 Tomita, H. and Tanaka, R.: Ocean surface warming and cooling responses and feedback
931 processes associated with polar lows over the Nordic seas, J. Geophys. Res. Atmospheres,
932 129, e2023JD040460, https://doi.org/10.1029/2023JD040460, 2024.

933 Tous, M. and Romero, R. D.-:10. 1002/joc. 3428: Meteorological environments associated with
934 medicane development, Int. J. Climatol., 33, 1–14, 2013.

935 Velez-Pardo, M. and Cronin, T. W.: Large-scale circulations and dry tropical cyclones in direct
936 numerical simulations of rotating Rayleigh-Bénard convection, J. Atmospheric Sci.,
937 https://doi.org/10.1175/JAS-D-23-0018.1, 2023.

938 Yanase, W. and co-authors: Climatology of polar lows over the Sea of Japan using the JRA-55
939 reanalysis, J Clim., 29, 419–437, 2016.

940 Yarovaya, D. A., Efimov, V. V., Shokurov, M. V., Stanichnyi, S. V., and Barabanov, V. S.: A
941 quasitropical cyclone over the Black Sea: Observations and numerical simulation, Phys.
942 Oceanogr., 18, 154–167, https://doi.org/10.1007/s11110-008-9018-2, 2008.

943 Zhang, W., Villarini, G., Scoccimarro, E., and Napolitano, F.: Examining the precipitation
944 associated with medicanes in the high-resolution ERA-5 reanalysis data, Int. J. Climatol., 41,
945 E126–E132, https://doi.org/10.1002/joc.6669, 2021.

946 Zhang, Y., Meng, Z., Zhang, F., and Weng, Y.: Predictability of tropical cyclone intensity
947 evaluated through 5-yr forecasts with a convection-permitting regional-scale model in the
948 Atlantic basin, Wea Forecast., 29, 1003–1022, 2014.

949